iScience

CellPress
OPEN ACCESS

Article

Innexin hemichannel activation by *Microplitis bicoloratus* ecSOD monopolymer reduces ROS

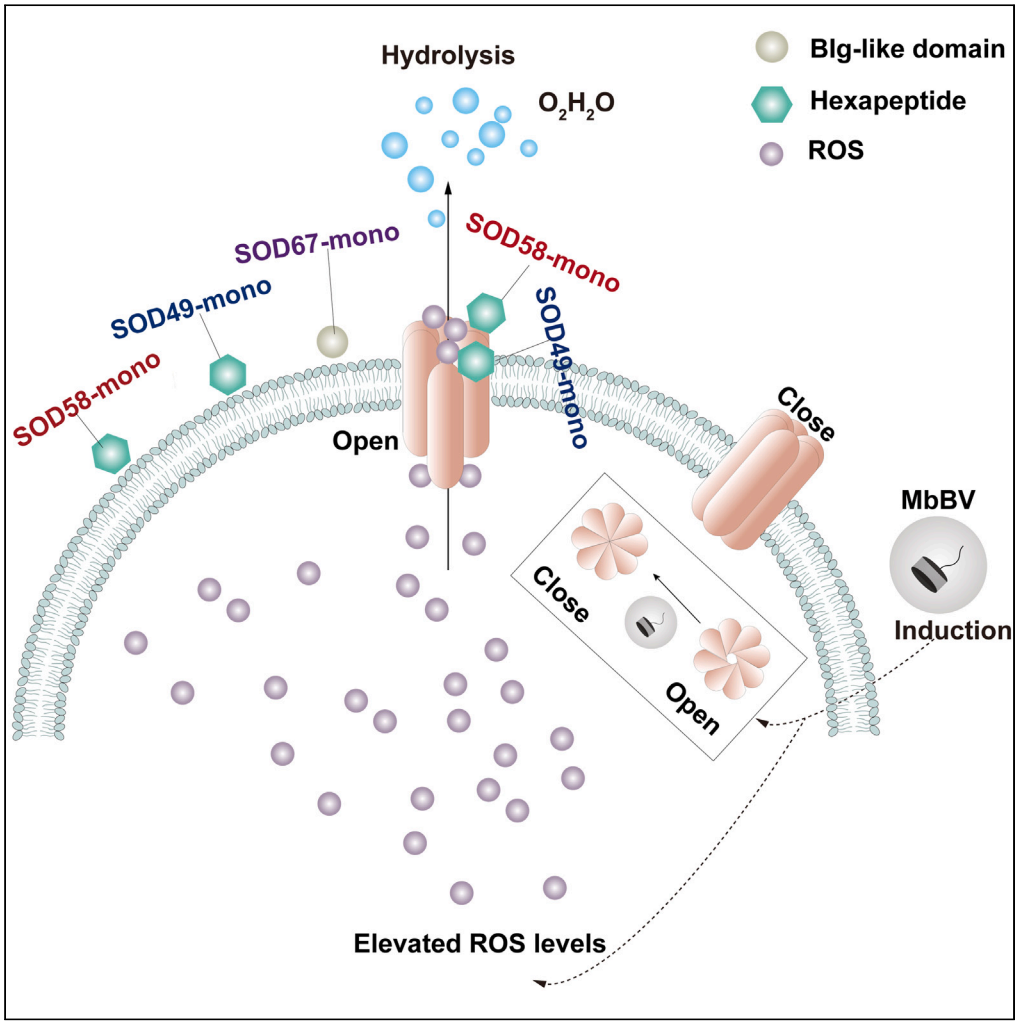

Jiang-Hui Meng, Yong-Biao Huang, Jin Long, ..., André F. Martins, Jean X. Jiang, Kai-Jun Luo

kaijun_luo@ynu.edu.cn

Highlights

EcSODs of *Microplitis bicoloratus* reduce ROS in host hemocytes

EcSODs monopolymers bind to the cell membrane to open hemichannels

EcSODs contain Ig beta-sandwiches with hexapep motif and Big-like domain

Hexapep motif and Big-like domain stabilize hemichannels via Inxs expression

Meng et al., iScience 27, 109469
April 19, 2024
https://doi.org/10.1016/j.isci.2024.109469

iScience

CellPress
OPEN ACCESS

Article

Innexin hemichannel activation by *Microplitis bicoloratus* ecSOD monopolymer reduces ROS

Jiang-Hui Meng,[1,2,3,7] Yong-Biao Huang,[1,2,3,7] Jin Long,[1,2,3,7] Qiu-Chen Cai,[4,5,7] Xin Qiao,[1,2,3,7] Qiong-Li Zhang,[1,2,3,7] Li-Dan Zhang,[6] Xiang Yan,[1,2,3] Rui Jing,[1,2,3] Xing-Shan Liu,[1,2,3] Sai-Jun Zhou,[1,2,3] Yong-Sheng Yuan,[1,2,3] Yin-Chen Ma,[1,2,3] Li-Xiang Zhou,[1,2,3] Nan-Nan Peng,[1,2,3] Xing-Cheng Li,[1,2,3] Cheng-Hui Cai,[1,2,3] Hong-Mei Tang,[1,2,3] André F. Martins,[4,5] Jean X. Jiang,[6] and Kai-Jun Luo[1,2,3,8,*]

SUMMARY

The extracellular superoxide dismutases (ecSODs) secreted by *Microplitis bicoloratus* reduce the reactive oxygen species (ROS) stimulated by the *Microplitis bicoloratus bracovirus*. Here, we demonstrate that the bacterial transferase hexapeptide (hexapep) motif and bacterial-immunoglobulin-like (Big-like) domain of ecSODs bind to the cell membrane and transiently open hemichannels, facilitating ROS reductions. RNAi-mediated ecSOD silencing *in vivo* elevated ROS in host hemocytes, impairing parasitoid larva development. *In vitro*, the ecSOD-monopolymer needed to be membrane bound to open hemichannels. Furthermore, the hexapep motif in the beta-sandwich of ecSOD49 and ecSOD58, and Big-like domain in the signal peptides of ecSOD67 were required for cell membrane binding. Hexapep motif and Big-like domain deletions induced ecSODs loss of adhesion and ROS reduction failure. The hexapep motif and Big-like domain mediated ecSOD binding via upregulating innexins and stabilizing the opened hemichannels. Our findings reveal a mechanism through which ecSOD reduces ROS, which may aid in developing anti-redox therapy.

INTRODUCTION

The extracellular superoxide dismutases (ecSODs) secreted by *Microplitis bicoloratus*, a parasitoid of *Spodoptera litura*, reduce the reactive oxygen species (ROS) stimulated by the *Microplitis bicoloratus bracovirus* (MbBV). However, the mechanism of how ecSODs reduce ROS is still unclear. *M. bicoloratus* secretes SODs to reduce ROS triggered by the symbiotic bracovirus MbBV and during infection of MbBV, cell-hemichannels are closed.[1,2] Understanding the closed hemichannel immunosuppression triggered by MbBV and the effects of the ecSODs in protecting parasitoid larval development against oxidative stress will provide essential insights into parasitoid-bracovirus-host interactions.

EcSODs exist widely across all living organisms in both hosts and pathogens. In humans, ecSODs are encoded by one sequence and can form two structures, a monomer and dimer[3]; ecSODs clear bacteria in the lungs by promoting phagocytosis.[4] In microbes, antioxidant enzymes, such as superoxide dismutase (SOD), transform ROS into less toxic products. The fungi *Fusarium oxysporum* secretes SOD5 to counteract the oxidative burst from the host plant's immune response.[5] *Leptopilina heterotoma*, a parasitoid of *Drosophila*, secretes ecSOD3, a monomeric glycosylated form found in its venom.[6] Anti-redox therapy is a protective mechanism that can be important for all living organisms.[7,8] Antioxidants are significant products of successful pathogens acting against ROS as a powerful deterrence against the anti-microbial mechanisms of the host.[9] Therefore, identifying the mechanisms by which ecSOD reduces intracellular ROS is a central challenge for their application in developing anti-redox therapy. Of course, ecSODs reduce ROS depending on cell binding properties and functional binding domains.

Hexapeptide (hexapep), a leader peptide of human recombinant manganese SOD, can enter cells and carry molecules, which can be considered a new molecular carrier.[10] Typically, human SOD3 is a secretory protein with a heparin-binding domain, with an affinity for heparin

[1]School of Life Sciences, Yunnan University, Kunming, Yunnan 650500, P.R. China
[2]Yunnan International Joint Laboratory of Virology & Immunology, Kunming, Yunnan 650500, P.R. China
[3]Key Laboratory of the University in Yunnan Province for International Cooperation in Intercellular Communications and Regulations, Yunnan University, Kunming, Yunnan 650500, P.R. China
[4]Werner Siemens Imaging Center, Department of Preclinical Imaging and Radiopharmacy, Eberhard Karls University Tübingen, 72076 Tübingen, Germany
[5]Cluster of Excellence iFIT (EXC 2180) "Image-Guided and Functionally Instructed Tumor Therapies", University of Tuebingen, 72076 Tübingen, Germany
[6]Department of Biochemistry and Structural Biology, University of Texas Health Science Center, San Antonio, TX 78229, USA
[7]These authors contributed equally
[8]Lead contact
*Correspondence: kaijun_luo@ynu.edu.cn
https://doi.org/10.1016/j.isci.2024.109469

proteoglycans on the cell surface and in the extracellular matrix, leading to the binding of SOD3 to the extracellular environment and cell membrane.[11–13] In contrast, in other species, the functional domains of ecSOD remain unclear. Proteins containing an immunoglobulin (Ig)-like domain vary in different functions, such as the Ig-like domain in hepatocyte cell adhesion molecule (hepaCAM) stabilizing the Cx43 hemichannels on the cell surface.[14] The bacterial-immunoglobulin-like (BIg-like) domains are involved in the innate-adaptive immune response with hemichannel/gap junction.[15]

Hemichannels are information channels with a role in substance exchange[16] and are mainly composed of innexins (Inxs), connexins (Cxs), and pannexins (Panxs).[17] Cxs are the key component of vertebrate gap junctions,[18] and Panx is distributed throughout the body. Inx proteins have the same topological structure as Cx and Panx proteins,[19] which are the structural elements of invertebrate hemichannels. Structurally, they consist of two extracellular rings (E1 and E2) and an intracellular ring, an amino and a carboxyl termini.[19] Functionally, a decrease in Inx transcription level or an increase in the amount of Inx proteins will affect the function of hemichannels; thus, the substance exchange via hemichannels depends on Inx homeostasis on the cell surface.[20]

Here, we showed that the hexapep motif and the BIg-like domain of ecSOD-mono are required for binding to the cell membrane and triggering Inx expression to stabilize hemichannels for the transient transportation of intracellular ROS to the extracellular environment, resulting in reduced ROS produced by the surrounding ecSODs. Our data revealed a specific function of the hexapep motif and BIg-like domain of ecSODs in reducing ROS in invertebrates. This uncovered a target for developing cell membrane binding-mediated ROS-reducers and candidate agents for developing broad anti-redox therapy.

RESULTS

EcSODs are required to reduce ROS and subsequently protect *M. bicoloratus* wasp development

To further understand parasitoids' self-protective mechanism via secretion of ecSODs,[1] hemocytes at different developmental stages were isolated, and the ROS levels were analyzed. In the embryo, 1st, 2nd, and 3rd instar larvae, the ROS levels in hemocytes were highly decreased compared with those in hemocytes from non-parasitoid larvae (Figure 1A). These results showed that ecSODs were secreted continuously in larvae (embryo to 3rd instar larvae), implying that ecSOD secretion accompanies the entire developmental stage of parasitoid larvae. We then determined whether an increase in ROS has a deleterious effect on wasp development. To this end, we established and used a host-parasitoid-double-stranded RNA (dsRNA) delivery system with which we silenced three ecSODs of *M. bicoloratus* (ecSOD49, ecSOD58, and ecSOD67 [ecCu/ZnSOD1]) (Figure S1A and S1B). The mRNA expression of *ecSODs* was significantly decreased after the dsRNA feeding (Figure 1B). After silencing the ecSODs of *M. bicoloratus*, the ROS in hemocytes significantly increased compared with the *egfp* dsRNA and control (Figure 1C). No effects on the host development were noted based on the head capsule width (Figure 1D) and parasitoid cocoon (Figure 1E); however, the eclosion of the wasp cocoon was significantly decreased (Figure 1F). These data showed that increased ROS resulted in a decreased eclosion of the parasitoid cocoons (Figure 1G), suggesting that ecSODs are required to reduce ROS to protect wasp development.

One sequence encodes two structures of ecSODs, a monopolymer and homodimer, in a cell-dependent manner

Petersen et al. reported that ecSOD has one sequence and two protein structures in humans.[3] We previously detected ecSODs in parasitized hemocytes with molecular weights of 18 and 35 kDa.[1] To further identify the structures of the ecSOD sequence, three ecSODs were expressed. Ectopic expression was performed in High Five cells that exhibited three ecSODs-V5-6His fusion proteins (~23 kDa for SOD49 and SOD67, ~24 kDa for SOD58) (Figure S2) in the cell pellets and cell condition medium (CM) (Figure 2A); furthermore, overexpression in *S. litura* Spli221 cells showed an additional faint ~40 kDa V5-6His fusion protein that was only present in the cell pellets (Figure 2B). These findings imply that the two structures of the ecSOD sequence are cell dependent. We named the two structures ecSOD monopolymer (ecSOD-mono) and ecSOD homodimer (ecSOD-dimer).

In the High Five cells, ecSOD-mono protein levels in the CM were the highest at 72 h compared with those at 24 and 48 h post-transfection (hpt) (Figure 2C). Conversely, intracellular protein levels presented a time-dependent decrease, as observed using immunofluorescence at 24, 48, and 72 hpt (Figure 2D). Thus, proteins inside the cells are expressed as polymers, and the monomer ecSOD-mono is secreted in a time-dependent manner into the extracellular space.

EcSODs monopolymers bind to the cell membrane to open hemichannels

The experimental procedure was further designed based on the secretion patterns of ecSODs (Figure 3A). The proteins collected from the initial transfected cells after 72 hpt were designated as CM A. Treatment of Spli221 cells with CM A resulted in decreased ROS levels induced by MbBV and carbenoxolone (CBX) (Figure S3A). Flow cytometry analysis revealed that three ecSODs CM A reduced the elevated ROS levels induced by MbBV. The ecSOD49 and ecSOD58 CM A also attenuated the increased ROS levels mediated by CBX (Figure 3B). These results showed that the secreted SODs (ecSOD49, ecSOD58, and ecSOD67) decreased the intracellular ROS. Furthermore, ~23 kDa proteins were present in pellet B and CM B of Spli221 cells incubated with CM A (Figures 3C–3E). Thus, ecSOD-mono was bound to the cell membrane. A faint presence of ecSOD-dimer proteins was also observed in Spli221 cells and pellets B, but not in CM B (Figures 3F–3H), indicating that a small amount of the dimer proteins also bound to the cell membrane. To further identify the localization of the monomers and homodimers of ecSOD on the cell membrane, membrane protein isolation was performed, with only the ~40 kDa dimer protein being successfully isolated (Figures 3I and 2K), suggesting that the homodimer was located deeper within the cell membrane. Furthermore, in Spli221 cells,

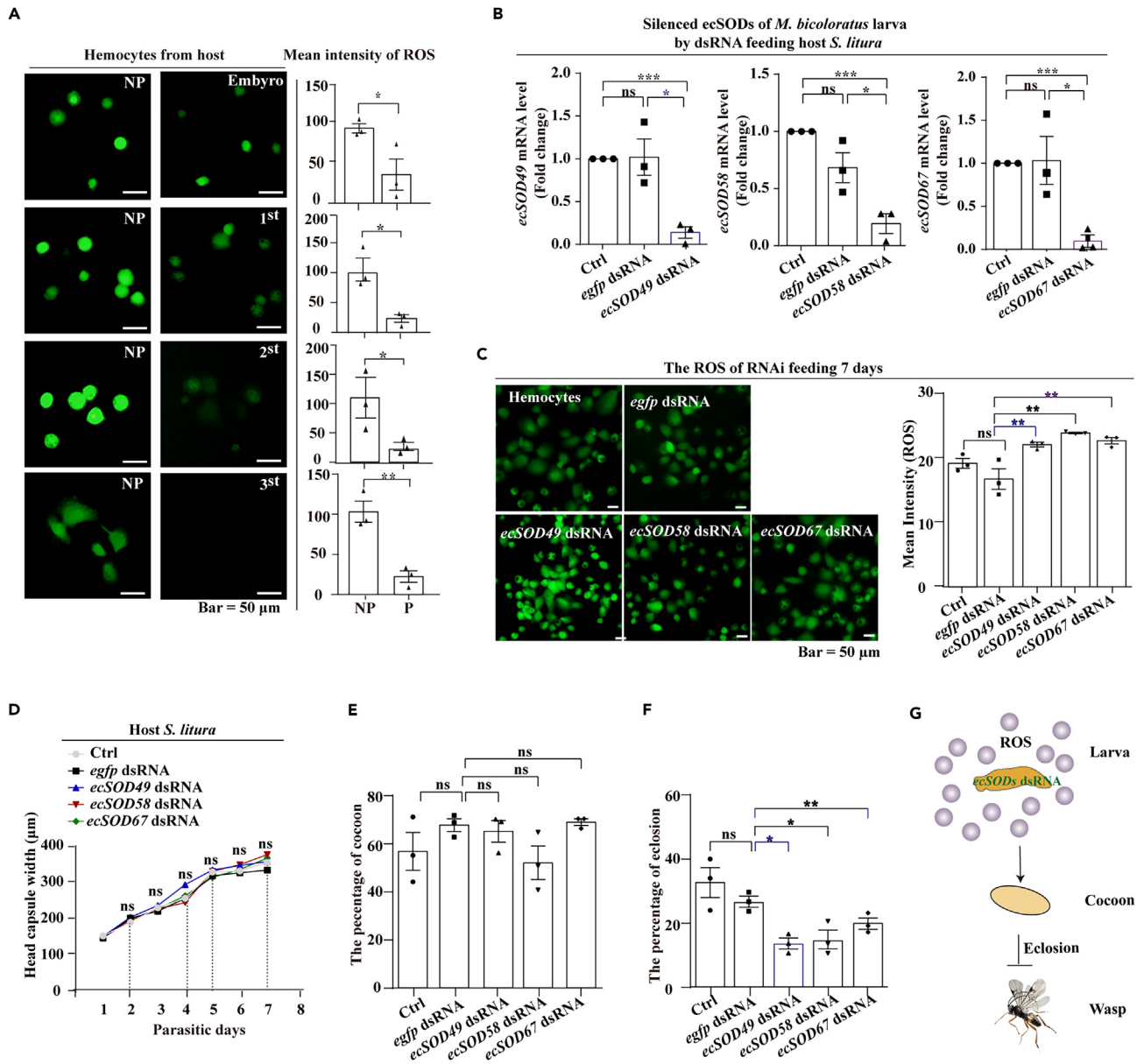

Figure 1. EcSODs are required to reduce ROS and subsequently protect *Microplitis bicoloratus* wasp development

(A) ROS detection in host hemocytes during the development of parasitoid *M. bicoloratus* larvae from embryo to 3rd larvae. NP: non-parasitized; 1st: the 1st larvae; 2nd: the 2nd larvae; 3rd: the 3rd larvae.Scale bar, 50 μm.

(B–F) Host-parasitoid-dsRNA delivery system silences the three ecSODs of parasitoid larvae individually. Graphs showing the qRT-PCR detection of the mRNA expression of the three ecSOD genes (B); ROS detection in host hemocytes treated with ecSOD dsRNA (C), Scale bar, 50 μm. ; the effect of ecSOD on the host development assessed using head capsule width during the development of parasitoid larvae (D); the percentage of parasitoid cocoons (E); the percentage of parasitoid eclosion (F).

(G) Illustration of the elevated ROS deleterious effect on wasp development. These data showed that increased ROS resulted in a decreased eclosion of the parasitoid cocoons, suggesting that ecSODs are required to reduce ROS to protect wasp development. See also Figure S1. In all graphs, data are represented as mean ± SEM. *$p < 0.05$, **$p < 0.01$, ***$p < 0.001$, ns, no significant differences. Unpaired Student's *t* test with Holm-Sidak method for multiple *t* test; n = 3.

hemichannels were closed via stimulation with MbBV and CBX, which are hemichannel inhibitors, showing that the subsequent administration of ecSODs CM A increased dye uptake by the cells (Figure 3L), suggesting that ecSOD acted by opening the hemichannels.

These results showed that both ecSOD structures act preferably at the cell membrane. The monopolymer ~23 kDa, which was abundant and bound to the extracellular surface of the membrane, reduced ROS via transiently opening hemichannels, while the less abundant

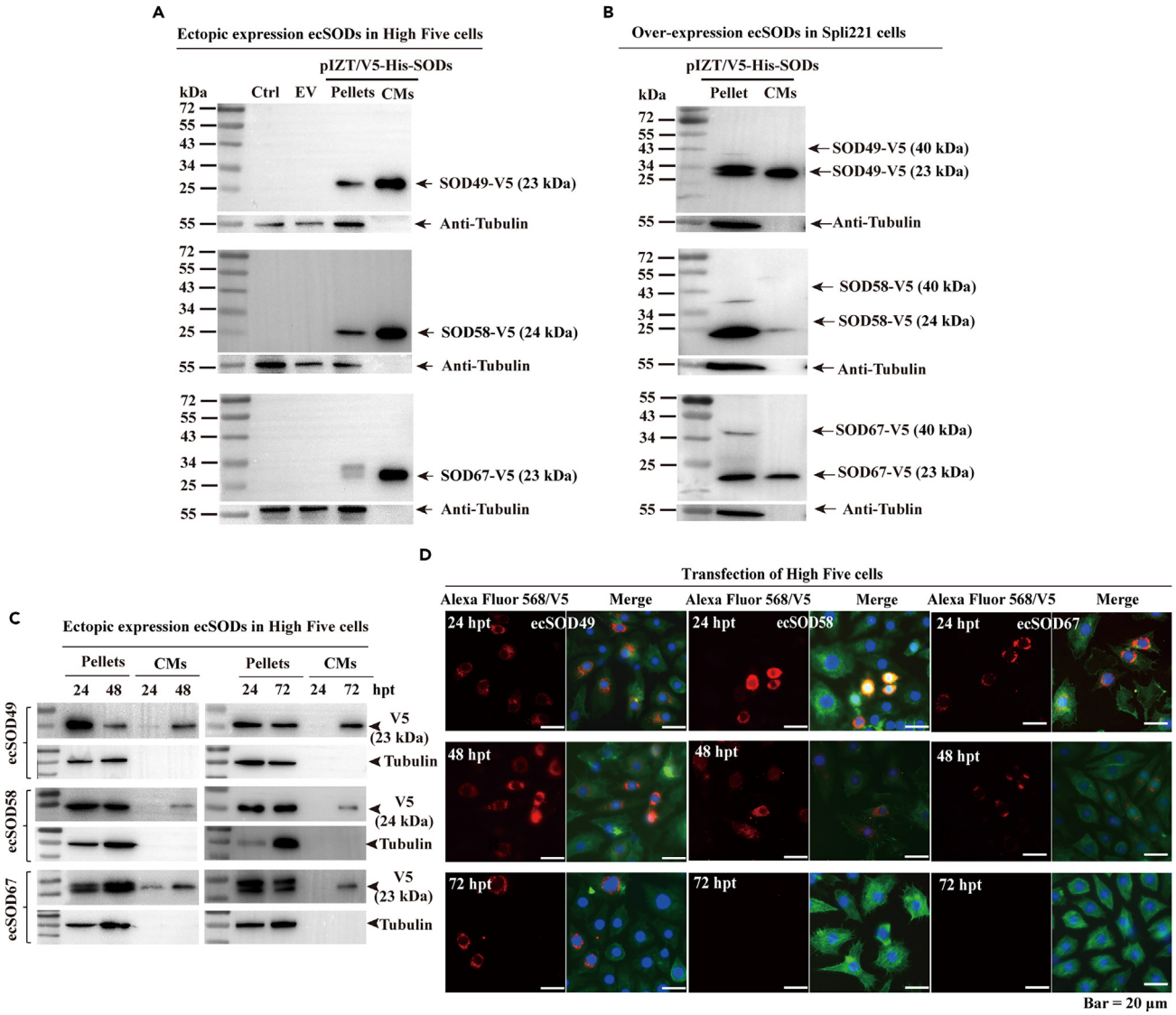

Figure 2. One sequence encodes two structures of ecSODs, a monopolymer and homodimer

(A) Ectopic expression of the three ecSODs in High Five cells; CMs: Condition mediums.

(B) Overexpression of the three ecSODs in host Spli221 cells; Red frame shows the ecSOD homodimer.

(C and D) The detection of the secreted pattern of ecSOD monopolymers in High Five cells at 24–72 h post-transfection (hpt). Intracellular and extracellular detection and localization of ecSODs using western blot (C) and immunofluorescence (D). Scale bar, 20 μm. See also Figure S2.

homodimer ~40 kDa may be part of the membrane proteins (Figure 3M). Thus, we further focused on studying the function of the ecSOD monopolymer in the cell membrane.

EcSOD bacterial transferase hexapep motif and BIg-like domain are required to be membrane bound to open hemichannels

Next, we elucidated how ecSODs bind to the cell membrane. We predicted the protein structures of three ecSODs. All ecSODs proteins contained an immunoglobulin beta-sandwich and signal peptide, implying that the three ecSODs belong to the secreted Ig-like family. The EcSOD49 and ecSOD58 proteins contain a bacterial transferase hexapep motif in the 9th (YSIIGRAVVVHSGV) and 7th (ISLVGTNNIGRGVVVHS) immunoglobulin beta-sandwiches, respectively (Figures 4A and 4B); ecSOD67 proteins contained a BIg-like) domain (KSIVILV) within the signal peptide (Figure 4C). We subcloned from ecSODs pIZT vectors and constructed ecSOD49$^{\Delta Hexapep}$, ecSOD58$^{\Delta Hexapep}$, and ecSOD67$^{\Delta BIg}$ via sequence alterations. ΔBIg of ecSOD67 was deleted without deleting the part of the signal peptide that facilitates its secretion (Figures S3A–S3C), and we predicted the molecular weight of the fused proteins, ecSOD49$^{\Delta Hexapep}$ (~21 kDa), ecSOD58$^{\Delta Hexapep}$, and ecSOD67$^{\Delta BIg}$ (~22 kDa), respectively (Figure S3D).

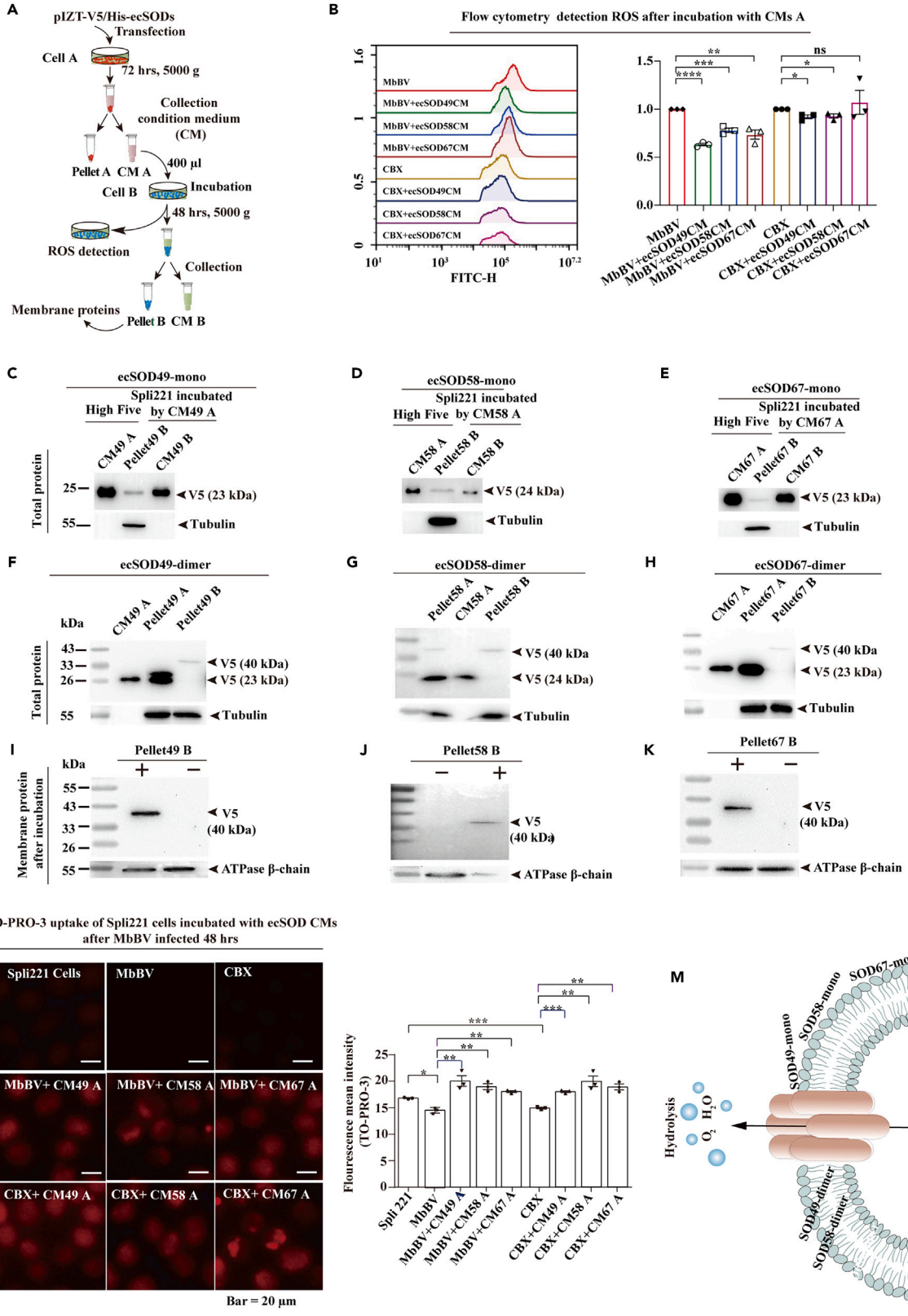
A
pIZT-V5/His-ecSODs
Transfection
Cell A
72 hrs, 5000 g
Collection
condition medium
(CM)
Pellet A CM A
400 µl
Cell B
Incubation
48 hrs, 5000 g
ROS detection
Collection
Membrane proteins
Pellet B CM B
B
Flow cytometry detection ROS after incubation with CMs A
MbBV
MbBV+ecSOD49CM
MbBV+ecSOD58CM
MbBV+ecSOD67CM
CBX
CBX+ecSOD49CM
CBX+ecSOD58CM
CBX+ecSOD67CM
FITC-H
ns
C
ecSOD49-mono
Spli221 incubated
High Five by CM49 A
CM49 A
Pellet49 B
CM49 B
Total protein
V5 (23 kDa)
Tubulin
D
ecSOD58-mono
Spli221 incubated
High Five by CM58 A
CM58 A
Pellet58 B
CM58 B
V5 (24 kDa)
Tubulin
E
ecSOD67-mono
Spli221 incubated
High Five by CM67 A
CM67 A
Pellet67 B
CM67 B
V5 (23 kDa)
Tubulin
F
ecSOD49-dimer
kDa
CM49 A
Pellet49 A
Pellet49 B
Total protein
V5 (40 kDa)
V5 (23 kDa)
Tubulin
G
ecSOD58-dimer
Pellet58 A
CM58 A
Pellet58 B
V5 (40 kDa
V5 (24 kDa)
Tubulin
H
ecSOD67-dimer
CM67 A
Pellet67 A
Pellet67 B
V5 (40 kDa
V5 (23 kDa)
Tubulin
I
Pellet49 B
kDa
Membrane protein
after incubation
V5
(40 kDa)
ATPase β-chain
J
Pellet58 B
V5
(40 kDa)
ATPase β-chain
K
Pellet67 B
V5
(40 kDa)
ATPase β-chain
L
TO-PRO-3 uptake of Spli221 cells incubated with ecSOD CMs
after MbBV infected 48 hrs
Spli221 Cells
MbBV
CBX
MbBV+ CM49 A
MbBV+ CM58 A
MbBV+ CM67 A
CBX+ CM49 A
CBX+ CM58 A
CBX+ CM67 A
Bar = 20 µm
Flourescence mean intensity
(TO-PRO-3)
Spli 221
MbBV
MbBV+CM49 A
MbBV+CM58 A
MbBV+CM67 A
CBX
CBX+CM49 A
CBX+CM58 A
CBX+CM67 A
M
SOD67-mono
SOD58-mono
SOD49-mono
Hydrolysis
SOD49-dimer
SOD58-dimer

Figure 3. EcSOD monopolymers bind to cell surface to open hemichannels

(A) Illustration of the experimental procedure of the collection of CMs A and B.

(B) Flow cytometry analysis of ROS in Spli221 cells at 48 h post-infection (hpi) triggered by MbBV and CBX treatment in the presence of CMs A.

(C–E) Membrane binding detection of ecSOD monopolymers in the Spli221 cells incubated with three CMs A: ecSOD49-mono (C), ecSOD58-mono (D), and ecSOD67-mono (E).

(F–H) Membrane binding detection of ecSOD homodimers in the Spli221 cells incubated with three CMs A: ecSOD49-dimer (F), ecSOD58-dimer (G), and ecSOD67-dimer (H).

(I–K) The localization of bound ecSODs on the cell surface by using membrane protein isolation: ecSOD49 (I), ecSOD58 (J), and ecSOD67 (K).

(L) Hemichannel detection in Spli221 cells triggered by MbBV and CBX incubation with CMs A by TO-PRO-3 uptake. Scale bar, 20 μm.

(M) Illustration of ecSOD bound to the cell surface and a hemichannel opened to reduce ROS. These data showed that ecSOD monopolymers bind to cell surface to open hemichannels, suggesting that membrane binding of ecSODs is required to reduce ROS. See also Figure S3. In all graphs, data are represented as mean ± SEM. *$p < 0.05$, **$p < 0.01$, ***$p < 0.001$, ****$p < 0.0001$, ns, no significant differences. Unpaired Student's *t* test with Holm-Sidak method for multiple *t* test; n = 3.

The deletion of hexapep motifs (Δhexapep) showed that ecSOD49$^{\Delta hexapep}$ presented as a normal 21 kDa protein expressed in cell pellet A and CM A in High Five cells. However, no 21 kDa ecSOD49$^{\Delta hexapep}$-mono protein was detected in the ecSOD49$^{\Delta hexapep}$ pellet B compared with the ecSOD49 pellet B on the cell surface of Spli221 cells incubated with CM49 A. Furthermore, membrane protein isolation also did not show any enrichment of ecSOD49$^{\Delta hexapep}$-dimer proteins compared with the ecSOD49-dimer proteins (Figures 4D and 4E). Similarly, ecSOD58$^{\Delta hexapep}$ resulted in the loss of the ecSOD58$^{\Delta hexapep}$-mono and -dimer proteins on the cell surface of Spli221 cells incubated with CM A (Figures 4F and 4G). The deletion of ecSOD67 Ig-like domain (ΔBIg) from the signal peptide showed normal secretion of the proteins in the High Five cells. Furthermore, ecSOD67$^{\Delta BIg}$ resulted in the loss of the ecSOD67$^{\Delta BIg}$-mono and -dimer on the cell surface of Spli221 cells incubated with CM A (Figures 4H and 4I). These results suggest that the loss of the hexapep motif and BIg-like domain resulted in the loss of the binding function on the cell surface. Importantly, flow cytometry showed that administrations of CM A to cells containing EcSOD49$^{\Delta hexapep}$, ecSOD58$^{\Delta hexapep}$, and ecSOD67$^{\Delta BIg}$ failed to reduce the ROS in Spli221 cells during MbBV treatment, contrasting compared with the typical functionality observed in the three ecSODs (Figures 4J and S4E). Thus, the hexapep motif and BIg-like domain are required for the membrane binding required to reduce ROS subsequently. Furthermore, the treatment with CM A of EcSOD49$^{\Delta hexapep}$, ecSOD58$^{\Delta hexapep}$, and ecSOD67$^{\Delta BIg}$ failed to open the hemichannels compared with the treatment with CM A of the three normal ecSODs (Figure 4K). In conclusion, the loss of the hexapep motif and BIg-like domain resulted in the loss of membrane binding and hemichannel opening (Figure 4L), implying that the hexapep motif and BIg-like domain are required for ecSODs to bind to the cell membrane and open the hemichannels.

EcSOD-mono hexapep motif and BIg-like domain upregulated the expression of Inxs and stability of hemichannels

We next examined how the hexapep motif and BIg-like domain facilitated the opening of the hemichannels. Because mutations of the Ig-like domain of hepaCAM were shown to decrease Cx43 via destabilizing Cx43,[21] we analyzed the expression and stability of Inxs. We hypothesized that the ecSOD regulated Inxs. To exclude ecSODs-dimer, which was only present on the Spli221 cells, paracrine/autocrine-ecSODs assays were performed in High Five cells to detect Inx expression after 72 hpt, when most of the ecSODs-mono was secreted. EcSODs-mono significantly increased the expression of four Inxs compared with those in the control groups; however, ecSODs$^{\Delta Hexapep}$ and ecSOD$^{\Delta BIg}$ resulted in a significantly decreased expression of Inx3 and Inx4 compared with that of the control groups. Notably, ecSODs$^{\Delta Hexapep}$ and ecSOD$^{\Delta BIg}$ significantly decreased the expression of Inx3 and Inx4 compared with ecSODs (Figures 5A and 5B). Furthermore, we determined whether ecSODs interacted with Inx3 and Inx4. Co-immunoprecipitation assays were performed and showed no interaction between the three SODs and Inx3 (Figures 5C–5F) or Inx4 (Figures 5G–5J), respectively. Parallel immunofluorescence assays showed that in the High Five cells incubated with CM A, the three ecSODs were significantly co-localized with Inx3 and Inx4 on the cell membranes (Figure 5K). Together with the findings presented in Figure 3, this showed that ecSODs-mono was bound on the cell surface, and the hexapep motif and BIg-like domain upregulated the expression of Inxs, implying that ecSODs transiently opened and stabilized hemichannels, which subsequently facilitated the reduction of ROS (Figure 5L).

EcSOD3-hexapep from invertebrates is an ancestor of the ecSOD3-HB domain from vertebrates, unlike the BIg-like domain

In invertebrates, ecSODs contain a hexapep motif, while in vertebrates, they contain a heparin-binding (HB) domain at the C terminus.[22–25] To explore whether ecSODs from the invertebrate *M. bicoloratus* can be applied to vertebrates to reduce ROS, we performed a sequence alignment of 28 different ecSOD3s from 25 different species, including *M. bicoloratus* and *Homo sapiens*. The results showed that the hexapep motif of the invertebrate ecSOD3 and the HB domain of the vertebrate ecSOD3 are highly conserved (Figure 6A). However, the cores of the hexapep motif and HB domains are different, especially at the proteins' C terminus (Figures 6B and 6C), which may determine the different binding sites of ecSOD3. Furthermore, a phylogenetic tree for homology analysis showed that the hexapep motif and HB domain containing ecSODs belong to two branches, and that the hexapep motif was present earlier in the phylogenetic tree than the HB domain. Notably, SOD1 from *H. sapiens* was more closely related to the invertebrate hexapep motif domains of wasps (*M. bicoloratus*, *M. demolitor*, *Cotesia chilonis*, *B. moris*, and *Caenorhabditis elegans*) (Figure 6D). The data showed that the ecSOD3 hexapep motif from invertebrates was an ancestor of the ecSOD3-HB domain from vertebrates, implying that the ecSOD containing the hexapep motif domain can be used in vertebrate species

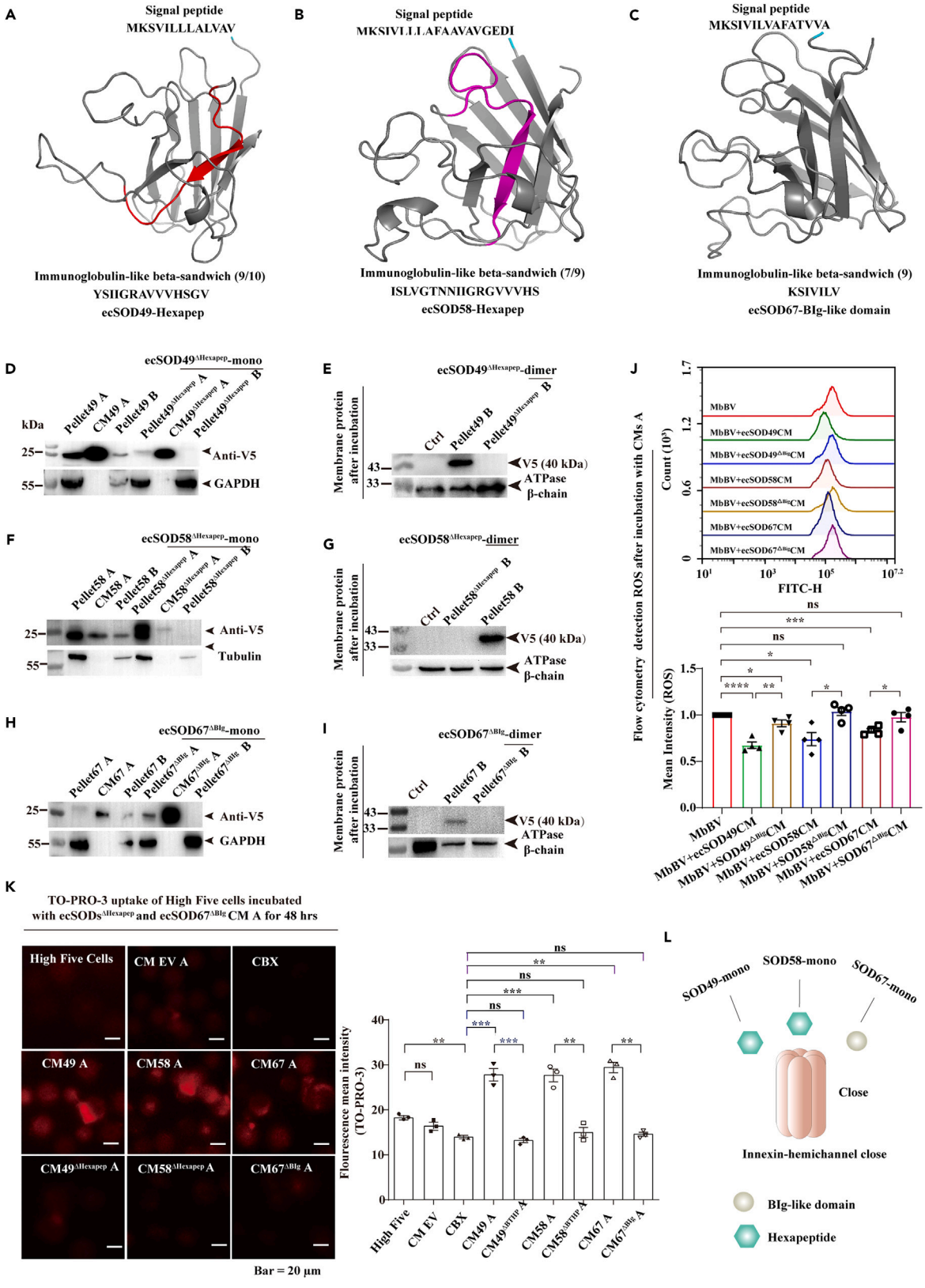
A
Signal peptide
MKSVILLLALVAV
Immunoglobulin-like beta-sandwich (9/10)
YSIIGRAVVVHSGV
ecSOD49-Hexapep
B
Signal peptide
MKSIVLILAFAAVAVGEDI
Immunoglobulin-like beta-sandwich (7/9)
ISLVGTNNIIGRGVVVHS
ecSOD58-Hexapep
C
Signal peptide
MKSIVILVAFATVVA
Immunoglobulin-like beta-sandwich (9)
KSIVILV
ecSOD67-BIg-like domain
D
ecSOD49ΔHexapep-mono
kDa
Pellet49 A
CM49 A
Pellet49 B
Pellet49ΔHexapep A
CM49ΔHexapep A
Pellet49ΔHexapep B
25
55
Anti-V5
GAPDH
E
ecSOD49ΔHexapep-dimer
Membrane protein after incubation
Ctrl
Pellet49 B
Pellet49ΔHexapep B
43
33
V5 (40 kDa)
ATPase
β-chain
F
ecSOD58ΔHexapep-mono
Pellet58 A
CM58 A
Pellet58 B
Pellet58ΔHexapep A
CM58ΔHexapep A
Pellet58ΔHexapep B
Anti-V5
Tubulin
G
ecSOD58ΔHexapep-dimer
Ctrl
Pellet58ΔHexapep B
Pellet58 B
H
ecSOD67ΔBIg-mono
Pellet67 A
CM67 A
Pellet67 B
Pellet67ΔBIg A
CM67ΔBIg A
Pellet67ΔBIg B
Anti-V5
GAPDH
I
ecSOD67ΔBIg-dimer
Ctrl
Pellet67 B
Pellet67ΔBIg B
J
Flow cytometry detection ROS after incubation with CMs A
MbBV
MbBV+ecSOD49CM
MbBV+ecSOD49ΔBigCM
MbBV+ecSOD58CM
MbBV+ecSOD58ΔBigCM
MbBV+ecSOD67CM
MbBV+ecSOD67ΔBigCM
Count (10³)
FITC-H
Mean Intensity (ROS)
MbBV+ecSOD49ΔBigCM
MbBV+ecSOD58ΔBigCM
MbBV+ecSOD67ΔBigCM
K
TO-PRO-3 uptake of High Five cells incubated with ecSODsΔHexapep and ecSOD67ΔBIg CM A for 48 hrs
High Five Cells
CM EV A
CBX
CM49 A
CM58 A
CM67 A
CM49ΔHexapep A
CM58ΔHexapep A
CM67ΔBIg A
Bar = 20 μm
Flourescence mean intensity (TO-PRO-3)
High Five
CM EV
CBX
CM49 A
CM49ΔHexapep A
CM58 A
CM58ΔHexapep A
CM67 A
CM67ΔBIg A
L
SOD49-mono
SOD58-mono
SOD67-mono
Close
Innexin-hemichannel close
BIg-like domain
Hexapeptide

Figure 4. EcSOD bacterial transferase hexapep motif and BIg-like domain are required for cell membrane binding to reduce ROS

(A–C) The predicted structures of three ecSODs, ecSOD49 (A), ecSOD58 (B), and ecSOD67 (C); red shows the hexapeptide motif of ecSOD49, purple shows the hexapeptide motif of ecSOD58, orange shows the BIg-like domain of ecSDO67, and green shows the signal peptide.

(D–F) The detection of membrane-bound ecSODs-mono deleted hexapep motif and BIg-like domain: ecSOD49$^{\Delta Hexapep}$ (D), ecSOD58$^{\Delta Hexapep}$ (E), and ecSOD67$^{\Delta BIg}$ (F).

(G–I) The detection of membrane-bound ecSODs-dimer deleted hexapep motif and BIg-like domain: ecSOD49$^{\Delta Hexapep}$ (G), ecSOD58$^{\Delta Hexapep}$ (H), and ecSOD67$^{\Delta BIg}$ (I).

(J) Flow cytometry analysis of ROS in Spli221 cells at 48 h post-infection (hpi) following incubation with MbBV, CM49$^{\Delta Hexapep}$ A, CM58$^{\Delta Hexapep}$ A, and CM67$^{\Delta BIg}$ A.

(K) Hemichannel detection in Spli221 cells triggered with CM49 A and CM49$^{\Delta Hexapep}$ A, CM58 A and CM58$^{\Delta Hexapep}$ A, and CM67A and CM67$^{\Delta BIg}$ A by To-PRO-3 uptake. Scale bar, 20 μm.

(L) Illustration of hemichannel closing after loss of the hexapep motif and BIg-like domain. These data showed that the deleted hexapep motif and BIg-like domain of ecSODs lost membrane binding function, suggesting that hexapep motif and BIg-like domain are required for cell membrane binding to reduce ROS. See also Figure S4. In all graphs, data are represented as mean ± SEM. *$p < 0.05$, **$p < 0.01$, ***$p < 0.001$, ns, no significant differences. Unpaired Student's *t* test with Holm-Sidak method for multiple *t* test; n = 3.

to reduce ROS. In contrast, the BIg-like domain within the signal peptide is unique to ecSOD67, and the sequence presented low conservation (Figures S4A and S4B). Thus, *M. bicoloratus* ecSODs presented a unique function of reducing ROS.

DISCUSSION

EcSODs are scavengers of biological ROS in the extracellular space. We aimed to study how cells facilitate ROS release into the extracellular environment and why ROS are not reduced before being released extracellularly. Herein, we tested the hypothesis that ecSOD binds to the cell membrane to open hemichannels, leading to the release and subsequent reduction of intracellular ROS. This is the first report regarding the involvement of the hexapep motif and BIg-like domain of ecSOD in mediating the efficient and safe reduction of ROS. Data suggest that this is a new insight into how invertebrate ecSODs could be used for further research on anti-redox therapies.

In previous studies, we suggested that the regulation of cellular immune response is linked to the opening and closing of hemichannels. When hemichannel closure is compromised, it leads to elevated ROS levels, causing host cell apoptosis and immunosuppression to protect the host cell against *M. bicoloratus* development. Conversely, an open hemichannel inhibits host cell apoptosis and immune response, thereby thwarting the development of M. bicoloratus.

EcSODs transiently open hemichannels to release intracellular ROS, which may be a new strategy against the hemichannel-closed immunosuppression mediated by MbBV. Under the stimulation of MbBV, Inxs typically downregulate and hemichannels close.[2] However, in this study, we have observed that ecSODs upregulate Inxs. Many transcription factors, such as NRF2, NF-κB, HIF1α, and FOXO, can be influenced by ROS, and we hypothesize that EcSOD may influence heparinase expression by inhibiting the activation of redox-sensitive transcription factors involved in regulating heparinase transcription, including Egr1, nuclear factor-nB, and Ets1/2, as reported previously by Teoh et al. Recently, we have shown that the ecSOD-mono hexapep motif and BIg-like domain upregulated the expression of Inxs, implying that exSOD triggered ROS transcription signaling pathways. The increased Inx expression leads to enhanced hemichannel stability.[21,26–28] Although further work is needed to show how ecSOD regulates Inx expression, enhancing stability, data suggest that ecSOD reduces the activation of ROS-blocked transcription factors that regulate Inxs transcription, like Dip3. In the presence of ecSODs, the hexapep motif and BIg-like domain were bound to the cell membrane and triggered the upregulation of Inx protein. Under oxidative stress, Cx43 hemichannels in mouse lens epithelial HLE-B3 cells opened and mediated the exchange of oxidants and antioxidants to facilitate the reduction of intracellular ROS.[29] Hemichannel opening is related to the regulation of intracellular ROS.

Furthermore, ecSODs bind to the cell surface as the first step prior to reducing intracellular ROS. In vertebrate ecSOD3, the HB domain is the main binding domain[12,13,30–34]; although the hexapep motif is also present in the sequence of ecSOD3, only a few studies have analyzed it. In invertebrate ecSODs, the HB domain could not be found, while the hexapep motif was found to perform a binding function.

Hexapep is an ancient cell membrane-binding motif found throughout the ecSOD3 phylogenic tree. The hexapep motif was extensively conserved in all species, from bacteria to humans and maintained its cell surface-binding function.[35–46] The human hexapep in the leading peptide rMnSOD synthesized in the cytoplasm embeds into the mitochondrial matrix via its leading sequence.[10,47] Here, we reported that the hexapep motif of ecSODs stabilized the opened hemichannels via binding to the cell surface. Further interesting questions remain to be answered, such as when and how the HB domain of ecSOD superseded the hexapep motif and whether the hexapep motif lost its function in the vertebrate ecSODs.

The BIg-like domain within the signaling peptide performed a binding function, a new finding regarding the function of ecSODs. Typically, signal peptides of immature ecSODs are cleaved after being secreted into the extracellular space; furthermore, the matured ecSOD gains enhanced protein stability via the glycosylation of asparagine.[47,48] In human cytomegalovirus, viral signal peptides can function as a protein-integral effector domain via a slow cleavage.[49] In *Bombyx mori nucleopolyhedrovirus* mature virions, the membrane fusion protein GP64 is secreted into the plasma membrane, retaining its signal peptide, which is required for infection.[50–52] Here, we found that the signal peptides containing BIg-like domains performed the cell membrane-binding function and were not cleaved. The cleavage efficiency was related to the length of the signal peptides; when the C terminus of the signal peptide was more prolonged than nine residues, the cleavage efficiency decreased, and no cleavage was observed when the C terminus was 13 residues long.[22,53] Using the Signal IP 5.0,[23] we found that in all three ecSOD cleavage sites, the C terminus was longer than 13 residues. We assumed that the longer C terminus of ecSODs may be

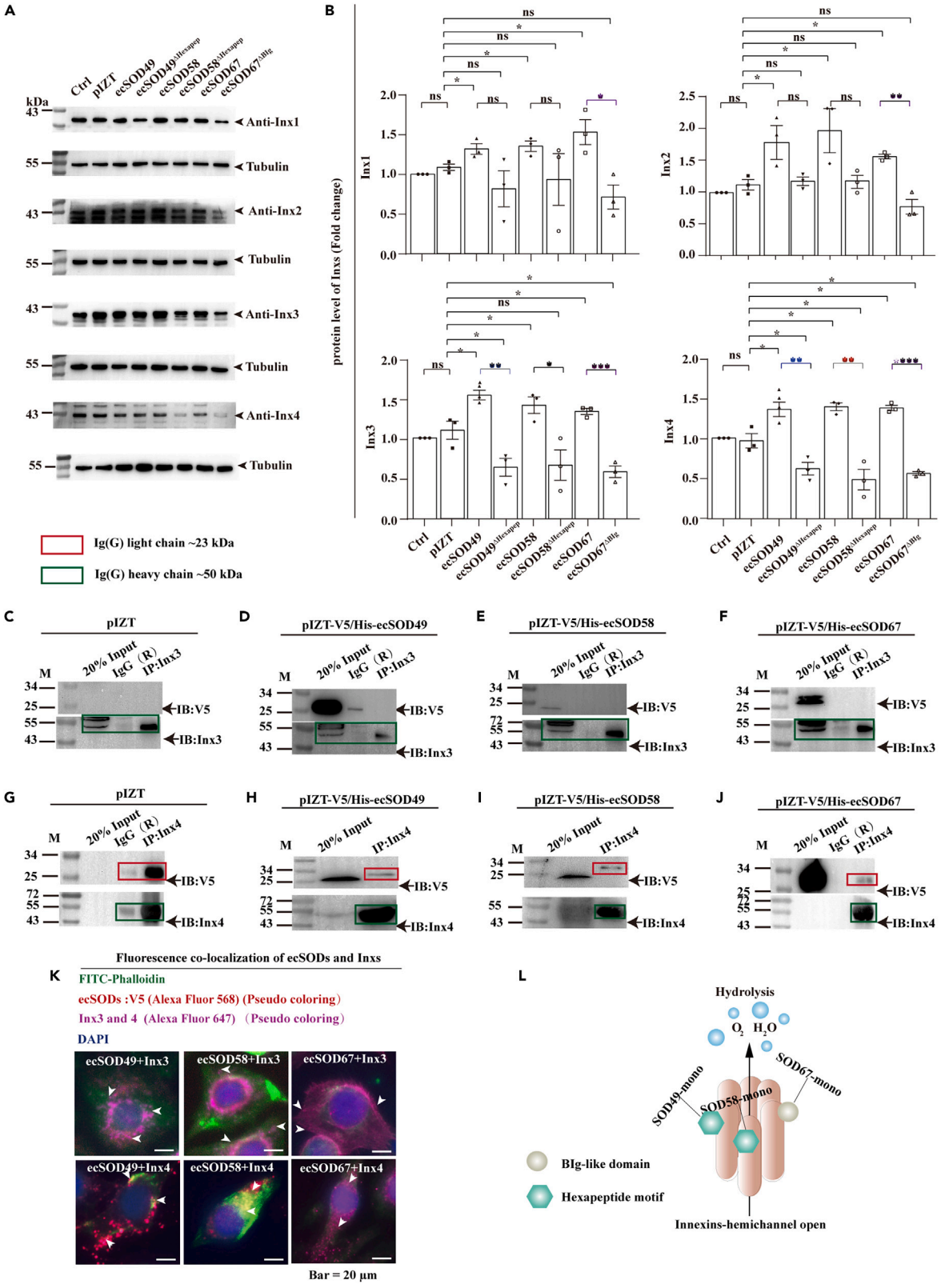
A
Ctrl
pIZT
ecSOD49
ecSOD49 6Hexapep
ecSOD58
ecSOD58 6Hexapep
ecSOD67
ecSOD67 3BIg
kDa
43
Anti-Inx1
55
Tubulin
43
Anti-Inx2
55
Tubulin
43
Anti-Inx3
55
Tubulin
43
Anti-Inx4
55
Tubulin
Ig(G) light chain ~23 kDa
Ig(G) heavy chain ~50 kDa
B
protein level of Inxs (Fold change)
Inx1
Inx2
Inx3
Inx4
ns
C
pIZT
D
pIZT-V5/His-ecSOD49
E
pIZT-V5/His-ecSOD58
F
pIZT-V5/His-ecSOD67
M
20% Input
IgG (R)
IP:Inx3
IB:V5
IB:Inx3
G
pIZT
H
pIZT-V5/His-ecSOD49
I
pIZT-V5/His-ecSOD58
J
pIZT-V5/His-ecSOD67
IP:Inx4
IB:Inx4
K
Fluorescence co-localization of ecSODs and Inxs
FITC-Phalloidin
ecSODs :V5 (Alexa Fluor 568) (Pseudo coloring)
Inx3 and 4 (Alexa Fluor 647) (Pseudo coloring)
DAPI
ecSOD49+Inx3
ecSOD58+Inx3
ecSOD67+Inx3
ecSOD49+Inx4
ecSOD58+Inx4
ecSOD67+Inx4
Bar = 20 μm
L
Hydrolysis
O2 H2O
SOD49-mono
SOD58-mono
SOD67-mono
BIg-like domain
Hexapeptide motif
Innexins-hemichannel open

Figure 5. EcSOD hexapep motif and BIg-like domain upregulated the expression of Inxs and stability of hemichannels

(A and B) The expressive levels of the four host Inxs, Inx1, Inx2, Inx3, and Inx4, in High Five cells with the expression of ecSODs and ecSODs$^{\Delta}$ via western blot.

(C–F) Interaction of Inx3 with the three ecSODs: control empty vector (C), ecSOD49 (D), ecSOD58 (E), and ecSOD67 (F).

(G–J) Interaction of Inx4 with the three ecSODs: control empty vector (G), ecSOD49 (H), ecSOD58 (I), and ecSOD67 (J).

(K) Colocalization of ecSODs with Inx3 and Inx4. Scale bar, 20 μm.

(L) Illustration of ecSOD stability in opened hemichannel to reduce ROS via hexapep motif and BIg-like domain, which upregulates Inxs. These data showed that hexapep motif and BIg-like domain are required for in opened-hemichannel to reduce ROS. In all graphs, data are represented as mean ± SEM. *$p < 0.05$, **$p < 0.01$, ***$p < 0.001$, ****$p < 0.0001$, ns, no significant differences. Unpaired Student's *t* test with Holm-Sidak method for multiple *t* test; n = 3.

disruptive to the cleavage, which remains a valuable question for further investigation. The Ig-like domain[24] exists in humans and can regulate the localization of the Cx43 protein on the membrane, and it is known to promote the occurrence of tumors.[21] The Ig-like domain found in hepaCAM is necessary to target intra- and intercellular interactions and play a role in the function of hemichannels.[21,25] The Ig-like domain in hepaCAM stabilizes Cx43 hemichannels. HepaCAM is differentially expressed in human hepatocellular carcinoma and regulates cell adhesion and motility.[14,54] In addition, cell surface localization and dimer formation were not affected by the deletion of the cytoplasmic domain of hepaCAM.[54] Here, the BIg-like domain stabilized hemichannels.

As a key protein in antioxidant research, SOD3 is widely involved in various molecular mechanisms and vital in signal regulation[55] and transduction. SOD3 can promote cartilage regeneration and is essential for normal pulmonary vascular development. Furthermore, an increased serum SOD3 expression and activity may prevent experimental bronchial dysplasia and lung injury in pulmonary hypertension.[11] It is worth noting that while other chemical scavengers can also contribute to ROS production, the mechanism of action of SODs is precise, catalyzing the conversion of superoxide radicals to hydrogen peroxide, which is then broken down into water and oxygen by other enzymes.[56,57]

EcSOD3 contains two copper ions, which may find application in positron emission tomography (PET) imaging of tumors when labeled with radioactive[64] Cu. In addition, ecSOD3 can effectively degrade extracellular and intracellular ROS; thus, using contrasting agents that bind to ROS specifically[59,60] can make ecSOD3 an efficient reporter protein for MRI. In conclusion, due to the high conservation between invertebrate and vertebrate ecSOD3, *M. bicoloratus* ecSOD3 can not only be an effective potential tumor therapy but can also become a good reporter protein for non-invasive imaging, such as MRI and PET.

In our study, the expression of Inxs was upregulated, and the hemichannels opened under the stimulation of ecSODs, which antagonized the closure of hemichannels stimulated by MbBV. Thus, a relationship among ecSODs, MbBV, and hemichannels is proposed. ROS reduction by ecSOD is one of the most essential immunosuppressive functions in parasitoid-bracovirus-host interactions. This is a potential key mechanism in the development of antioxidant therapies.

Limitations of the study

Our data are primarily based on the parasitoid-bracovirus-host interaction in immune responses. Although we confirmed that the hexapep motif and BIg-like domain of ecSODs transiently open hemichannels to reduce ROS, regulating the retained signal peptide of ecSODs may promote hemichannels. Given that the novel "retained signal peptide opening hemichannel" model proposes the global regulation between membrane fusion and hemichannel opening and closure in immune responses, further investigation will be necessary to fully understand the molecular mechanisms underlying the link between cellular ROS-ecSOD-hemichannel immunity during MbBV infection.

STAR★METHODS

Detailed methods are provided in the online version of this paper and include the following:

- KEY RESOURCES TABLE
- RESOURCE AVAILABILITY
  - Lead contact
  - Materials availability
- EXPERIMENTAL MODEL AND SUBJECT DETAILS
  - Cell lines
  - Insect rearing
  - Microplitis bicoloratus bracovirus (MbBV)
- METHOD DETAILS
  - Isolation of hemocytes from larvae of *S. litura*
  - ROS detection
  - Flow cytometry analysis of intracellular ROS
  - Plasmid construction and expression
  - Plasmid construction for dsRNA feeding
  - Preparation of dsRNA and dsRNA feeding
  - Western blotting
  - Real-time qRT-PCR
  - Immunofluorescence

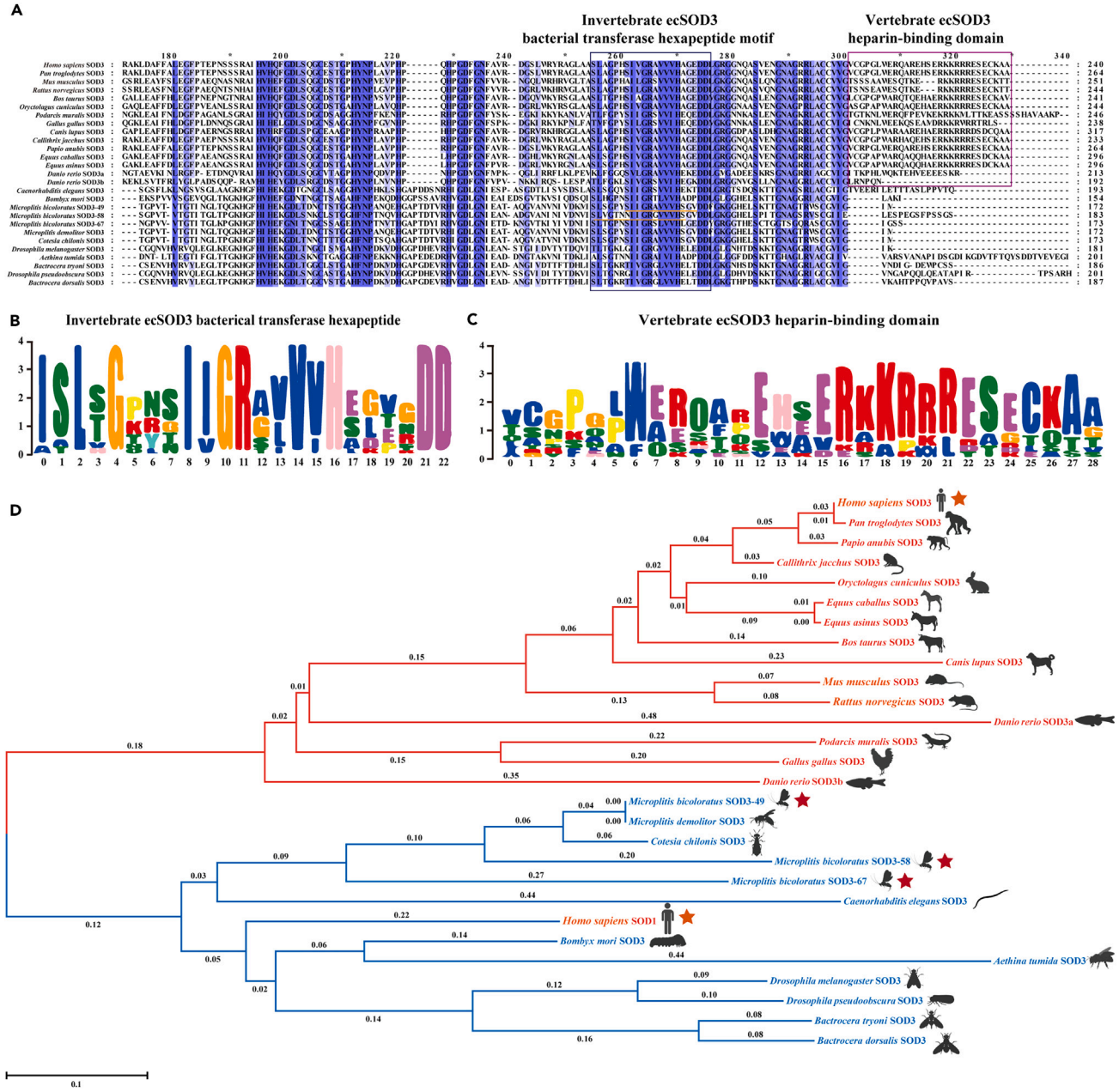

Invertebrate ecSOD3 containing bacterical transferase hexapeptide motif (hexapep motif)

Vertebrate ecSOD3 containing heparin-binding domain (HB domain)

Figure 6. EcSOD3 hexapep from invertebrates is an ancestor of the ecSOD3-HB domain from vertebrates, unlike the BIg-like domain

(A) The invertebrate ecSOD3 hexapep motif and the vertebrate ecSOD3-HB domain are highly conserved according to the sequence alignment; red frame shows hexapep motif, green frame shows the deleterious region, and rose frame shows the heparin-binding domain.

(B) The core sequences of invertebrate ecSOD3 hexapep motifs are LxGxxxIIGRAVVVHxxxDD.

(C) The core sequences of vertebrate ecSOD3-HB domains are SxxNGNAGxRLACxVxG.

(D) Neighbor joining of the phylogenetic tree of ecSOD3 is depicted, and according to the degree of variation, the hexapeptide motif and HB domain containing ecSODs belong to two branches. See also Figure S5.

- Dye uptake via hemichannels
- Detection of proteins in the cell membrane
- Co-immunoprecipitation and immunoblot assay
- Prediction of functional domains
- Neighbor joining (NJ) phylogenetic tree construction

- QUANTIFICATION AND STATISTICAL ANALYSIS

SUPPLEMENTAL INFORMATION

Supplemental information can be found online at https://doi.org/10.1016/j.isci.2024.109469.

ACKNOWLEDGMENTS

We would like to thank everyone who assisted with the preparation of this manuscript. This work was supported by the National Natural Science Foundation of China (grant numbers 32160662, 31772225, 31471823, 31260448, and 31060251), the Science and Technology Planning Project in Key Areas of Yunnan Province (grant number 202001BB050002), NSFC-NRF (grant number 31411140238 to K.-J.L.), and Yunnan Department of Science and Technology (grant number 2013FA003 to K.-J.L.). K.-J.L. was supported by the Donglu Scholar Program of Yunnan University.

AUTHOR CONTRIBUTIONS

Conceptualization, K.-J.L., J.-H.M., Y.-B.H., J.L., X.Q., Q.-C.C., A.F.M., and J.X.J.; methodology, K.-J.L., J.-H.M., Y.-B.H., J.L., X.Q., L.-D.Z., and Q.C.C.; investigation, J.-H.M., Y.-B.H., J.L., X.Q., L.-D.Z., Q.-C.C., Q.-L.Z., X.Y., R.J., X.-S.L., S.-J.Z., Y.-S.Y., Y.-C.M., X.Q., L.-X.Z., X.-C.L., N.-N.P., C.-H.C., and H.-M.T.; visualization, J.-H.M., J.L., Y.-B.H., L.-D.Z., and Q.-C.C.; funding acquisition, K.-J.L.; project administration, K.-J.L.; supervision, K.-J.L., A.F.M., and J.X.J.; writing – original draft, K.-J.L., J.-H.M., J.L., Y.-B.H., L.-D.Z., and Q.-C.C.; writing – review and editing, K.-J.L., J.-H.M., J.L., Y.-B.H., L.-D.Z., Q.-C.C., A.F.M., and J.X.J.

DECLARATION OF INTERESTS

The authors declare no competing interests.

Received: July 14, 2023
Revised: January 31, 2024
Accepted: March 7, 2024
Published: March 18, 2024

REFERENCES

1. Zhang, L.D., Cai, Q.C., Cui, J.H., Zhang, W., Dong, S.M., Xiao, W., Li, J., Kou, T.C., Zhang, X.W., He, H.J., et al. (2019). A secreted-Cu/Zn superoxide dismutase from Microplitis bicoloratus reduces reactive oxygen species triggered by symbiotic bracovirus. Dev. Comp. Immunol. *92*, 129–139. https://doi.org/10.1016/j.dci.2018.11.014.
2. Chen, C.X., He, H.J., Cai, Q.C., Zhang, W., Kou, T.C., Zhang, X.W., You, S., Chen, Y.B., Liu, T., Xiao, W., et al. (2021). Bracovirus-mediated innexin hemichannel closure in cell disassembly. iScience *24*, 102281. https://doi.org/10.1016/j.isci.2021.102281.
3. Petersen, S.V., Oury, T.D., Valnickova, Z., Thøgersen, I.B., Højrup, P., Crapo, J.D., and Enghild, J.J. (2003). The dual nature of human extracellular superoxide dismutase: one sequence and two structures. Proc. Natl. Acad. Sci. USA *100*, 13875–13880. https://doi.org/10.1073/pnas.2436143100.
4. Manni, M.L., Tomai, L.P., Norris, C.A., Thomas, L.M., Kelley, E.E., Salter, R.D., Crapo, J.D., Chang, L.Y.L., Watkins, S.C., Piganelli, J.D., and Oury, T.D. (2011). Extracellular superoxide dismutase in macrophages augments bacterial killing by promoting phagocytosis. Am. J. Pathol. *178*, 2752–2759. https://doi.org/10.1016/j.ajpath.2011.02.007.
5. Wang, Q., Pokhrel, A., and Coleman, J.J. (2021). The extracellular superoxide dismutase Sod5 from *Fusarium oxysporum* is localized in response to external stimuli and contributes to fungal pathogenicity. Front. Plant Sci. *12*, 608861. https://doi.org/10.3389/fpls.2021.608861.
6. Colinet, D., Cazes, D., Belghazi, M., Gatti, J.L., and Poirié, M. (2011). Extracellular superoxide dismutase in insects: characterization, function, and interspecific variation in parasitoid wasp venom. J. Biol. Chem. *286*, 40110–40121. https://doi.org/10.1074/jbc.M111.288845.
7. Kolar, S.L., and Liu, G.Y. (2017). RAS and ROS—A story of *Pseudomonas* survival. Cell Host Microbe *21*, 551–552. https://doi.org/10.1016/j.chom.2017.04.009.
8. Hussain, S.S., and Kashatus, D.F. (2018). MDVs: Spare the SOD and spoil the bug. Cell Host Microbe *24*, 616–618. https://doi.org/10.1016/j.chom.2018.10.013.
9. Vareechon, C., Zmina, S.E., Karmakar, M., Pearlman, E., and Rietsch, A. (2017). *Pseudomonas aeruginosa* effector ExoS inhibits ROS production in human neutrophils. Cell Host Microbe *21*, 611–618.e5. https://doi.org/10.1016/j.chom.2017.04.001.
10. Borrelli, A., Schiattarella, A., Mancini, R., Pica, A., Pollio, M.L., Ruggiero, M.G., Bonelli, P., De Luca, V., Tuccillo, F.M., Capasso, C., et al. (2016). A new hexapeptide from the leader peptide of rMnSOD enters cells through the oestrogen receptor to deliver therapeutic molecules. Sci. Rep. *6*, 18691. https://doi.org/10.1038/srep18691.
11. Sherlock, L.G., Trumpie, A., Hernandez-Lagunas, L., McKenna, S., Fisher, S., Bowler, R., Wright, C.J., Delaney, C., and Nozik-Grayck, E. (2018). Redistribution of extracellular superoxide dismutase causes neonatal pulmonary vascular remodeling and PH but protects against experimental bronchopulmonary dysplasia. Antioxidants *7*, 42. https://doi.org/10.3390/antiox7030042.
12. Tibell, L.A., Sethson, I., and Buevich, A.V. (1997). Characterization of the heparin-binding domain of human extracellular superoxide dismutase. Biochim. Biophys. Acta *1340*, 21–32. https://doi.org/10.1016/s0167-4838(97)00024-1.
13. Enghild, J.J., Thogersen, I.B., Oury, T.D., Valnickova, Z., Hojrup, P., and Crapo, J.D. (1999). The heparin-binding domain of extracellular superoxide dismutase is proteolytically processed intracellularly during biosynthesis. J. Biol. Chem. *274*, 14818–14822.

14. Favre-Kontula, L., Rolland, A., Bernasconi, L., Karmirantzou, M., Power, C., Antonsson, B., and Boschert, U. (2008). GlialCAM, an immunoglobulin-like cell adhesion molecule is expressed in glial cells of the central nervous system. Glia *56*, 633–645. https://doi.org/10.1002/glia.20640.
15. Meng, J.-H., Chen, C.-X., Ahmadian, M.R., Zan, H., Luo, K.-J., and Jiang, J.X. (2022). Cross-activation of hemichannels/gap junctions and immunoglobulin-like domains in innate–adaptive immune responses. Front. Immunol. *13*, 882706. https://doi.org/10.3389/fimmu.2022.882706.
16. Dahl, G., and Muller, K.J. (2014). Innexin and pannexin channels and their signaling. FEBS Lett. *588*, 1396–1402. https://doi.org/10.1016/j.febslet.2014.03.007.
17. Skerrett, I.M., and Williams, J.B. (2017). A structural and functional comparison of gap junction channels composed of connexins and innexins. Dev. Neurobiol. *77*, 522–547. https://doi.org/10.1002/dneu.22447.
18. Yen, M.R., and Saier, M.H., Jr. (2007). Gap junctional proteins of animals: the innexin/pannexin superfamily. Prog. Biophys. Mol. Biol. *94*, 5–14. https://doi.org/10.1016/j.pbiomolbio.2007.03.006.
19. Beyer, E.C., and Berthoud, V.M. (2018). Gap junction gene and protein families: Connexins, innexins, and pannexins. Biochim. Biophys. Acta. Biomembr. *1860*, 5–8. https://doi.org/10.1016/j.bbamem.2017.05.016.
20. Pang, Z., Li, M., Yu, D., Yan, Z., Liu, X., Ji, X., Yang, Y., Hu, J., and Luo, K. (2015). TWO INNEXINS OF Spodoptera litura INFLUENCES HEMICHANNEL AND GAP JUNCTION FUNCTIONS IN CELLULAR IMMUNE RESPONSES. Arch. Insect Biochem. Physiol. *90*, 43–57. https://doi.org/10.1002/arch.21243.
21. Wu, M., Moh, M.C., and Schwarz, H. (2016). HepaCAM associates with connexin 43 and enhances its localization in cellular junctions. Sci. Rep. *6*, 36218. https://doi.org/10.1038/srep36218.
22. Jain, R.G., Rusch, S.L., and Kendall, D.A. (1994). Signal peptide cleavage regions Functional limits on length and topological implications. J. Biol. Chem. *269*, 16305–16310.
23. Teufel, F., Almagro Armenteros, J.J., Johansen, A.R., Gíslason, M.H., Pihl, S.I., Tsirigos, K.D., Winther, O., Brunak, S., von Heijne, G., and Nielsen, H. (2022). SignalP 6.0 predicts all five types of signal peptides using protein language models. Nat. Biotechnol. *40*, 1023–1025. https://doi.org/10.1038/s41587-021-01156-3.
24. Mei, S., Zhang, J., Zhang, X., and Tu, X. (2015). Solution structure of a bacterial immunoglobulin-like domain of the outer membrane protein (LigB) from Leptospira. Proteins *83*, 195–200. https://doi.org/10.1002/prot.24723.
25. Tan, B., Tan, J., Du, H., Quan, Z., Xu, X., Jiang, X., Luo, C., and Wu, X. (2014). HepaCAM inhibits clear cell renal carcinoma 786-0 cell proliferation via blocking PKC epsilon translocation from cytoplasm to plasma membrane. Mol. Cell. Biochem. *391*, 95–102. https://doi.org/10.1007/s11010-014-1991-9.
26. Cai, Q.-C., Chen, C.-X., Liu, H.-Y., Zhang, W., Han, Y.-F., Zhang, Q., Zhou, G.-F., Xu, S., Liu, T., Xiao, W., et al. (2021). Interactions of Vank proteins from *Microplitis bicoloratus bracovirus* with host Dip3 suppress eIF4E expression. Dev. Comp. Immunol. *118*, 103994. https://doi.org/10.1016/j.dci.2021.103994.
27. Lennicke, C., and Cochemé, H.M. (2021). Redox metabolism: ROS as specific molecular regulators of cell signaling and function. Mol. Cell *81*, 3691–3707. https://doi.org/10.1016/j.molcel.2021.08.018.
28. Teoh, M.L.T., Fitzgerald, M.P., Oberley, L.W., and Domann, F.E. (2009). Overexpression of extracellular superoxide dismutase attenuates heparanase expression and inhibits breast carcinoma cell growth and invasion. Cancer Res. *69*, 6355–6363. https://doi.org/10.1158/0008-5472.Can-09-1195.
29. Quan, Y., Du, Y., Wu, C., Gu, S., and Jiang, J.X. (2021). Connexin hemichannels regulate redox potential via metabolite exchange and protect lens against cellular oxidative damage. Redox Biol. *46*, 102102. https://doi.org/10.1016/j.redox.2021.102102.
30. Chu, Y., Piper, R., Richardson, S., Watanabe, Y., Patel, P., and Heistad, D.D. (2006). Endocytosis of extracellular superoxide dismutase into endothelial cells: role of the heparin-binding domain. Arterioscler. Thromb. Vasc. Biol. *26*, 1985–1990. https://doi.org/10.1161/01.ATV.0000234921.88489.5c.
31. Stenlund, P., Lindberg, M.J., and Tibell, L.A.E. (2002). Structural requirements for high-affinity heparin binding: alanine scanning analysis of charged residues in the C-terminal domain of human extracellular superoxide dismutase. Biochemistry *41*, 3168–3175. https://doi.org/10.1021/bi011454r.
32. Chu, Y., Iida, S., Lund, D.D., Weiss, R.M., DiBona, G.F., Watanabe, Y., Faraci, F.M., and Heistad, D.D. (2003). Gene transfer of extracellular superoxide dismutase reduces arterial pressure in spontaneously hypertensive rats: role of heparin-binding domain. Circ. Res. *92*, 461–468. https://doi.org/10.1161/01.RES.0000057755.02845.F9.
33. Sandström, J., Nilsson, P., Karlsson, K., and Marklund, S.L. (1994). 10-fold increase in human plasma extracellular superoxide dismutase content caused by a mutation in heparin-binding domain. J. Biol. Chem. *269*, 19163–19166.
34. Sandström, J., Carlsson, L., Marklund, S.L., and Edlund, T. (1992). The heparin-binding domain of extracellular superoxide dismutase C and formation of variants with reduced heparin affinity. J. Biol. Chem. *267*, 18205–18209. https://doi.org/10.1016/s0021-9258(19)37173-x.
35. Egan, S.A., Kurian, D., Ward, P.N., Hunt, L., and Leigh, J.A. (2010). Identification of sortase A (SrtA) substrates in Streptococcus uberis: evidence for an additional hexapeptide (LPXXXD) sorting motif. J. Proteome Res. *9*, 1088–1095. https://doi.org/10.1021/pr901025w.
36. Chang, Q., Zhang, L., He, C., Zhang, B., Zhang, J., Liu, B., Zeng, N., and Zhu, Z. (2015). HOXB9 induction of mesenchymal-to-epithelial transition in gastric carcinoma is negatively regulated by its hexapeptide motif. Oncotarget *6*, 42838–42853. https://doi.org/10.18632/oncotarget.5814.
37. Macwan, A.S., Srivastava, N., Javed, S., and Kumar, A. (2013). Role of a repeated hexapeptide motif GIHFAP near C-terminus in assembly, stability, and activity of "HCH dehydrochlorinase LinA. Appl. Biochem. Biotechnol. *169*, 1397–1404. https://doi.org/10.1007/s12010-012-0035-8.
38. Canela, N., Orzáez, M., Fucho, R., Mateo, F., Gutierrez, R., Pineda-Lucena, A., Bachs, O., and Pérez-Payá, E. (2006). Identification of an hexapeptide that binds to a surface pocket in cyclin A and inhibits the catalytic activity of the complex cyclin-dependent kinase 2-cyclin A. J. Biol. Chem. *281*, 35942–35953.
39. Sano, K.-I., and Shiba, K. (2003). A hexapeptide motif that electrostatically binds to the surface of titanium. J. Am. Chem. Soc. *125*, 14234–14235. https://doi.org/10.1021/ja038414q.
40. Kundu, B., Srinivasan, T., Kesarwani, A.P., Kavishwar, A., Raghuwanshi, S.K., Batra, S., and Shukla, P.K. (2002). Identification of novel antifungal nonapeptides through the screening of combinatorial peptide libraries based on a hexapeptide motif. Bioorg. Med. Chem. Lett. *12*, 1473–1476. https://doi.org/10.1016/s0960-894x(02)00174-9.
41. Hammerschmidt, S., Tillig, M.P., Wolff, S., Vaerman, J.P., and Chhatwal, G.S. (2000). Species-specific binding of human secretory component to SpsA protein of Streptococcus pneumoniae via a hexapeptide motif. Mol. Microbiol. *36*, 726–736. https://doi.org/10.1046/j.1365-2958.2000.01897.x.
42. Chan, S.K., Pöpperl, H., Krumlauf, R., and Mann, R.S. (1996). An extradenticle-induced conformational change in a HOX protein overcomes an inhibitory function of the conserved hexapeptide motif. EMBO J. *15*, 2476–2487.
43. Radulescu, R.T., Bellitti, M.R., Ruvo, M., Cassani, G., and Fassina, G. (1995). Binding of the LXCXE insulin motif to a hexapeptide derived from retinoblastoma protein. Biochem. Biophys. Res. Commun. *206*, 97–102. https://doi.org/10.1006/bbrc.1995.1014.
44. Vuorio, R., Härkönen, T., Tolvanen, M., and Vaara, M. (1994). The novel hexapeptide motif found in the acyltransferases LpxA and LpxD of lipid A biosynthesis is conserved in various bacteria. FEBS Lett. *337*, 289–292. https://doi.org/10.1016/0014-5793(94)80211-4.
45. Inoue, K., and Odo, S. (1994). The adhesive protein cDNA of *Mytilus galloprovincialis* encodes decapeptide repeats but no hexapeptide motif. Biol. Bull. *186*, 349–355. https://doi.org/10.2307/1542281.
46. Antonsson, P., Heinegård, D., and Oldberg, A. (1989). The keratan sulfate-enriched region of bovine cartilage proteoglycan consists of a consecutively repeated hexapeptide motif. J. Biol. Chem. *264*, 16170–16173.
47. Ota, F., Kizuka, Y., Kitazume, S., Adachi, T., and Taniguchi, N. (2016). N-Glycosylation is essential for the secretion of extracellular superoxide dismutase. FEBS Lett. *590*, 3357–3367. https://doi.org/10.1002/1873-3468.12378.
48. Yan, Z., and Spaulding, H.R. (2020). Extracellular superoxide dismutase, a molecular transducer of health benefits of exercise. Redox Biol. *32*, 101508. https://doi.org/10.1016/j.redox.2020.101508.
49. Seidel, E., Dassa, L., Kahlon, S., Tirosh, B., Halenius, A., Seidel Malkinson, T., and Mandelboim, O. (2021). A slowly cleaved viral signal peptide acts as a protein-integral immune evasion domain. Nat. Commun. *12*, 2061. https://doi.org/10.1038/s41467-021-21983-x.
50. Hao, B., Liu, L., Liu, N., Sun, L., Fan, F., and Huang, J. (2022). The *Bombyx mori* nucleopolyhedrovirus GP64 retains the transmembrane helix of signal peptide to contribute to secretion across the cytomembrane. Microbiol. Spectr. *10*,

e0191322. https://doi.org/10.1128/spectrum.01913-22.

51. Hao, B., Nan, W., Xu, Y., Liu, L., Liu, N., and Huang, J. (2021). Two cholesterol recognition amino acid consensus motifs of GP64 with uncleaved signal peptide are required for *Bombyx mori* nucleopolyhedrovirus Infection. Microbiol. Spectr. *9*, e0172521. https://doi.org/10.1128/Spectrum.01725-21.
52. Yao, C., Pan, S., Xu, Y., Lu, M., Zhao, Y., Huo, J., Hao, B., and Huang, J. (2023). Bombyx mori Nucleopolyhedrovirus Hijacks Multivesicular Body as an Alternative Envelopment Platform for Budded Virus Egress. J. Virol. *97*, e0004123. https://doi.org/10.1128/jvi.00041-23.
53. Auclair, S.M., Bhanu, M.K., and Kendall, D.A. (2012). Signal peptidase I: cleaving the way to mature proteins. Protein Sci. *21*, 13–25. https://doi.org/10.1002/pro.757.
54. Chung Moh, M., Hoon Lee, L., and Shen, S. (2005). Cloning and characterization of hepaCAM, a novel Ig-like cell adhesion molecule suppressed in human hepatocellular carcinoma. J. Hepatol. *42*, 833–841. https://doi.org/10.1016/j.jhep.2005.01.025.
55. Li, M., Pang, Z., Xiao, W., Liu, X., Zhang, Y., Yu, D., Yang, M., Yang, Y., Hu, J., and Luo, K. (2014). A transcriptome analysis suggests apoptosis-related signaling pathways in hemocytes of *Spodoptera litura* after parasitization by *Microplitis bicoloratus*. PLoS One *9*, e110967. https://doi.org/10.1371/journal.pone.0110967.
56. Wang, Y., Branicky, R., Noë, A., and Hekimi, S. (2018). Superoxide dismutases: Dual roles in controlling ROS damage and regulating ROS signaling. J. Cell Biol. *217*, 1915–1928. https://doi.org/10.1083/jcb.201708007.
57. Karmakar, A., Das, A.K., Ghosh, N., and Sil, P.C. (2022). Chapter2.7 - Superoxide dismutase. In Antioxidants Effects in Health, S.M. Nabavi and A.S. Silva, eds. (Elsevier), pp. 139–166. https://doi.org/10.1016/B978-0-12-819096-8.00027-6.
58. Luo, K., Trumble, J.T., and Pang, Y. (2007). Development of *Microplitis bicoloratus* on *Spodoptera litura* and implications for biological control. BioControl *52*, 309–321. https://doi.org/10.1007/s10526-006-9030-8.
59. Fu, C., Herbst, S., Zhang, C., and Whittaker, A.K. (2017). Polymeric 19F MRI agents responsive to reactive oxygen species. Polym. Chem. *8*, 4585–4595. https://doi.org/10.1039/c7py00986k.
60. Tain, R.W., Scotti, A.M., and Cai, K. (2019). Improving the detection specificity of endogenous MRI for reactive oxygen species (ROS). J. Magn. Reson. Imaging. *50*, 583–591. https://doi.org/10.1002/jmri.26629.
61. Granados, R.R., Guoxun, L., Derksen, A.C., and McKenna, K.A. (1994). A new insect cell line from *Trichoplusia ni* (BTI-Tn-5B1-4) susceptible to *Trichoplusia ni* single enveloped nuclear polyhedrosis virus. J. Invertebr. Pathol. *64*, 260–266.
62. Vaughn, J.L., Goodwin, R.H., Tompkins, G.J., and McCawley, P. (1977). The establishment of two cell lines from the insect *Spodoptera frugiperda* (Lepidoptera; Noctuidae). In Vitro *13*, 213–217.
63. Yanase, T., Yasunaga, C., and Kawarabata, T. (1998). Replication of *Spodoptera exigua* nucleopolyhedrovirus in permissive and non-permissive lepidopteran cell lines. Acta Virol. *42*, 293–298.
64. Li, G.-H., Chen, Q.-J., and Pang, Y. (1998). Studies of artificial diets for the beet armyworm, Spodoptera exigua. Acta Scientiae Circumstan- tiae/Huanjing Kexue Xuebao *4*, 1–5.
65. Luo, K., and Pang, Y. (2006). Spodoptera litura multicapsid nucleopolyhedrovirus inhibits *Microplitis bicoloratus* polydnavirus-induced host granulocytes apoptosis. J. Insect Physiol. *52*, 795–806. https://doi.org/10.1016/j.jinsphys.2006.04.007.
66. Luo, K.-J., and Pang, Y. (2006). Disruption effect of *Microplitis bicoloratus* polydnavirus EGF-like protein, MbCRP, on actin cytoskeleton in lepidopteran insect hemocytes. Acta Biochim. Biophys. Sin. *38*, 577–585. https://doi.org/10.1111/j.1745-7270.2006.00195.x.
67. Liu, T., Li, M., Zhang, Y., Pang, Z., Xiao, W., Yang, Y., and Luo, K. (2013). A role for Innexin2 and Innexin3 proteins from *Spodoptera litura* in apoptosis. PLoS One *8*, e70456. https://doi.org/10.1371/journal.pone.0070456.
68. Timmons, L., Court, D.L., and Fire, A. (2001). Ingestion of bacterially expressed dsRNAs can produce specific and potent genetic interference in *Caenorhabditis elegans*. Gene *263*, 103–112.
69. Dong, S.M., Cui, J.H., Zhang, W., Zhang, X.W., Kou, T.C., Cai, Q.C., Xu, S., You, S., Yu, D.S., Ding, L., et al. (2017). Inhibition of translation initiation factor eIF4A is required for apoptosis mediated by *Microplitis bicoloratus bracovirus*. Arch. Insect Biochem. Physiol. *96*, e21423. https://doi.org/10.1002/arch.21423.
70. Livak, K.J., and Schmittgen, T.D. (2001). Analysis of relative gene expression data using real-time quantitative PCR and the $2^{-\Delta\Delta CT}$ method. Methods *25*, 402–408. https://doi.org/10.1006/meth.2001.1262.
71. Kou, T.C., Liu, Y.T., Li, M., Yang, Y., Zhang, W., Cui, J.H., Zhang, X.W., Dong, S.M., Xu, S., You, S., et al. (2017). Identification of beta-chain of Fo F1 -ATPase in apoptotic cell population induced by *Microplitis bicoloratus* bracovirus and its role in the development of *Spodoptera litura*. Arch. Insect Biochem. Physiol. *95*, e21389. https://doi.org/10.1002/arch.21389.
72. Sharma, S., Ciufo, S., Starchenko, E., Darji, D., Chlumsky, L., Karsch-Mizrachi, I., and Schoch, C.L. (2019). The NCBI BioCollections Database. Database *2019*, baz057. https://doi.org/10.1093/database/baz057.
73. Tippmann, H.F. (2004). Analysis for free: comparing programs for sequence analysis. Brief. Bioinform. *5*, 82–87. https://doi.org/10.1093/bib/5.1.82.
74. Kumar, S., Stecher, G., and Tamura, K. (2016). MEGA7: molecular evolutionary genetics analysis version 7.0 for bigger datasets. Mol. Biol. Evol. *33*, 1870–1874. https://doi.org/10.1093/molbev/msw054.
75. Crooks, G.E., Hon, G., Chandonia, J.M., and Brenner, S.E. (2004). WebLogo: a sequence logo generator. Genome Res. *14*, 1188–1190. https://doi.org/10.1101/gr.849004.

STAR★METHODS

KEY RESOURCES TABLE

REAGENT or RESOURCE	SOURCE	IDENTIFIER
Antibodies		
Mouse anti-Tubulin	Transgen Biotech	Cat#HC101: RRID: AB_2893358
Mouse anti-GAPDH	Transgen Biotech	Cat# HC301; RRID: AB_2629434
Mouse anti-V5	Invitrogen	Cat#R960-25; RRID:AB_2556564
Rabbit anti-ATPase β chain	GL Binchem synthesis	N/A
Rabbit anti-Inx1	GL Binchem synthesis	N/A
Rabbit anti-Inx2	GL Binchem synthesis	N/A
Rabbit anti-Inx3	GL Binchem synthesis	N/A
Rabbit anti-Inx4	GL Binchem synthesis	N/A
Alexa Fluor 647, Goat Anti-Rabbit IgG(H + L)	Beyotime	Cat#A0468
Alexa Fluor 568, Goat anti-Rabbit IgG (H + L)	Invitrogen	Cat#A-11011
Bacterial and plasmid		
DH5α	TaKaRa	Cat#9057
HT115	Self made	N/A
L4440	MiaolingBio	Cat#P0311
pBM16A	Biomed	Cat#CL071-01
pIZT	Self made	N/A
Chemicals, peptides, and recombinant proteins		
5×Protein SDS-PAGE Loading Buffer	Beyotime	Cat#PO286
Ampicillin, sodium salt	COOLABER	Cat#69-52-3
IPTG	Sigma	Cat#I6758
Native lysis Buffer	Solarbio	Cat#R0030
PMSF	Solarbio	Cat#P0100
Protein A-G Agarose	Beyotime	Cat#P2012
RIPA buffer (high)	Solarbio	Cat#R0010
Tetracycline HCL	BIOFROXX	Cat#1302GR005
Zeocin Antibiotic	Thermo Fisher	Cat#R250
PVDF	Millipore	Cat#IPVH00010
Tween 20	Solarbio	Cat#T8200
TEMED	DingGuo	Cat#DH338-1
Protein Ladder	Thermo Fisher	Cat#26617
TNM-FH	Procell	Cat#PM152010
RNAiso Plus	Takara Bio	Cat#9109
FBS	gibco	Cat#2350722RP
Binding Buffer	Self made	N/A
To-PRO-3	Invitrogen	Cat#T3605
Experimental models: Cell lines		
Spli221	Luo Lab stock	N/A
Sf9	Luo Lab stock	N/A
High Five	Luo Lab stock	N/A
Critical commercial assays		
Endo-free Plasmid Mini Kit II	OMEGA	Cat#D6950-01B

(*Continued on next page*)

Continued

REAGENT or RESOURCE	SOURCE	IDENTIFIER
Gel Extraction Kit	omega	Cat#D2500
Plasmid Mini Kit I	omega	Cat#D6943-02
BCA protein quantitative kit	DingGuo	Cat#BCA02
Reactive Oxygen Species Assay Kit	Beyotime	Cat#S0033S
Minute Plasma Membrane Protein Isolation and Cell Fractionation Kit	Invent	Cat#SM-005
Oligonucleotides		
pIZT- ecSOD49ΔHexapep-F-1: GGTACCATGAAATCAGTCATATTGC	This paper	N/A
pIZT- ecSOD49ΔHexapep-R-1: CAAAATCATCATATGGTCCAGATAGAGAG	This paper	N/A
pIZT- ecSOD49Δ Hexapep -F-2 TGGACCATATGATGATTTTGGTAAAGGAGG	This paper	N/A
pIZT- ecSOD49Δ Hexapep -R −2: GAATTCATAATTCCAATAACACCAC	This paper	N/A
pIZT- ecSOD58ΔHexapep -F-1: GGTACCATGAAATCAATCGTTTTA	Luo Lab stock	N/A
pIZT- ecSOD58ΔHexapep -R-1: CATCAACACCAATCACATTATCAACAATATTTATGTTAG	Luo Lab stock	N/A
pIZT- ecSOD58Δ Hexapep -F-2: TAATGTGATTGGTGTTGATGATCTCGGC	Luo Lab stock	N/A
pIZT- ecSOD58ΔHexapep -R-2: CCGCGGGTTGTAATATTTGA	Luo Lab stock	N/A
pIZT- ecSOD67ΔBIg-F-1: GGTACCATGGCCTTTGCCA	Luo Lab stock	N/A
pIZT- ecSOD67ΔBIg-R −1: GAATTCGAGGATCCGATTC	Luo Lab stock	N/A
pIZT/V5-His-ecSOD49-F: GGGGTACCATGAAATCAGTCATATTGCTG	Luo Lab stock	N/A
pIZT/V5-His-ecSOD49-R: CCGCTCGAGATGGTGATGGTGATGATGACCG	Luo Lab stock	N/A
pIZT/V5-His-ecSOD58-F: GGGGTACCATGAAATCAATCGTTTTATTGCTG	Luo Lab stock	N/A
pIZT/V5-His-ecSOD58-R: CCGCTCGAGATGGTGATGGTGATGATGACCGGT	Luo Lab stock	N/A
pIZT/V5-His-ecSOD67-F: GGGGTACCATGAAATCAATCGTTATATTAGTGGC	Luo Lab stock	N/A
pIZT/V5-His-ecSOD67-R: CCGCTCGAGATGGTGATGGTGATGATGAC	Luo Lab stock	N/A
qRT-PCR-MbSOD49-F: TCTAGAATGAAATCAGTCATATTGC	This paper	N/A
qRT-PCR-MbSOD49-R: GTCGACATAATTCCAATAACACCAC	This paper	N/A
qRT-PCR-MbSOD58-F: GGTACCATGAAATCAATCGTTTTA	This paper	N/A
qRT-PCR-MbSOD58-R: CCGCGGGTTGTAATATTTGA	This paper	N/A
qRT-PCR-MbSOD67-F: GCTCTAGAATGAAATCAATCGTTATA	This paper	N/A

(*Continued on next page*)

Continued

REAGENT or RESOURCE	SOURCE	IDENTIFIER
qRT-PCR-MbSOD67-R: CCCAAGCTTTTAAGAGGATCCG	This paper	N/A
pIZT-SOD49	This paper	N/A
pIZT-SOD58	This paper	N/A
pIZT-SOD67	This paper	N/A
pIZT-SOD49$^{\Delta Hexapep}$	This paper	N/A
pIZT-SOD58$^{\Delta Hexapep}$	This paper	N/A
pIZT-SOD67$^{\Delta Big}$	This paper	N/A
pIZT-Spil-Inx1	Luo Lab stock	N/A
pIZT-Spil-Inx2	Luo Lab stock	N/A
pIZT-Spil-Inx3	Luo Lab stock	N/A
pIZT-Spil-Inx4	Luo Lab stock	N/A
L4440-SOD49	This paper	N/A
L4440-SOD58	This paper	N/A
L4440-SOD67	This paper	N/A
L4440-eGFP	Luo Lab stock	N/A
Software and algorithms		
Prism8	Graphpad	https://www.graphpad.com
Premier5	Premie	N/A
ImageJ	ImageJ	https://imagej.nih.gov/ij/
SMART	SMART	http://smart.embl-heidelberg.de/
NCBI	NCBI	http://www.ncbi.nlm.nih.blast
HDOCK Server	HDOCK Server	HDOCK Server (hust.edu.cn)
Softberry	Softberry	SERVICES (softberry.com)

RESOURCE AVAILABILITY

Lead contact

Further information requests for resources and reagents should be directed to and will be fulfilled by the lead contact, Kai-Jun Luo (kaijun_luo@ynu.edu.cn).

Materials availability

This study did not generate new unique reagents.

EXPERIMENTAL MODEL AND SUBJECT DETAILS

Cell lines

High Five Cells were derived from *Trichoplusia*,[61] Sf9 (IPLB-Sf21-AE) cells were derived from *S. frugiperda* pupal ovarian tissue,[62] and adherent Spli221 (TUAT-Spli221) cells were derived from *S. litura*[63] cultured in TNM-FH insect culture medium supplemented with 10% fetal bovine serum (Hyclone, Logan, UT, USA).

Insect rearing

The *Spodoptera litura* colonies were grown on an artificial diet at 27 ± 1°C and 60–80% humidity.[64] The parasitoid *M. bicoloratus* colonies were maintained on *S. litura* larvae grown in the laboratory. Adults were provided with honey as a dietary supplement.[58]

Microplitis bicoloratus bracovirus (MbBV)

Purified viral particles were prepared based on a previously published protocol,[65,66] with minor modifications. Briefly, fresh wasps were frozen at −20°C for 10 min and then put on ice. Reproductive tracts of female wasps were excised under a binocular stereo dissecting microscope, and separated ovaries were collected into a 2-mL tube on ice until further use. The calyces were punctured using forceps, and the calyx fluid

was resuspended in 1x PBS, and then using a 2.5-mL needle, dispersed by aspirating back and forth. The mixture was centrifuged for 3 min at 1,000 × *g* at 4°C, to remove eggs and cellular debris. A 0.45-mL syringe filter was used to purify the viral particles.

METHOD DETAILS

Isolation of hemocytes from larvae of *S. litura*

Hemocytes were prepared based on a previously published protocol,[1,55] with minor modifications. Hemolymph (500 μL) isolated from ~100 larvae of *S. litura* was centrifuged at 4°C for 5 min at 1,000 × *g*, and pellets were collected as hemocytes. The pellets were centrifuged for 5 min at 1000 × *g*, washed with 1× phosphate-buffered saline (PBS) twice, and resuspended in 1 mL PBS. Next, 1 × 10^5 cells were added to each well of a 12-well plate. Hemocytes isolated from parasitized larvae were referred to as parasitized samples, and those from unparasitized larvae were used as controls.

ROS detection

ROS detection was performed based on a previously published protocol,[1] with minor modifications. A ROS detection kit (S0033S, Beytime, Shanghai, China) was used for ROS detection in hemocytes parasitized by *M. bicoloratus* and Spli221 cells infected with MbBV particles following the manufacturer's instructions. Briefly, 50 μL of hemolymph was isolated from ~50 larvae of *S. litura* parasitized by *M. bicoloratus* from the embryo to the 3rd larval stage. Next, 1 × 10^5 hemocytes were added in a dropwise manner into each well of a 24-well plate containing 100 μL serum-free medium for 5 min and then washed twice with serum-free medium. Thereafter, 0.1 μL DCFH-DA was added to each well at a final concentration of 10 μM. The cells were then incubated for 30 min at 37°C, washed twice with PBS, and imaged using an Olympus 71 inverted fluorescence microscope. ImageJ was used to measure the fluorescence intensity.

Flow cytometry analysis of intracellular ROS

1 × 10^5 Spli221 cells were implanted into 12-well plates. After treating the cells with MbBV and CBX for 48 h, the treated cells were incubated with a conditioned medium transfected with Mb-SODs mutated and unmutated domains for 24 h, and the cells were stained by the ROS Assay Kit (Beyotime; S0033S; Shanghai; China). Flow cytometry (NovoCyte Advanteon System; Agilent; Hangzhou; China) was used to assess the intracellular levels of reactive oxygen species (ROS) in cells.

Plasmid construction and expression

Plasmids were constructed as described previously,[67] with minor modifications. The genes were directionally cloned into the pBM16A vector (CL071-01, Biomed, Beijing, China), and the inserts were confirmed by direct sequencing. Finally, the eukaryotic expression plasmid pIZT/V5-His (Invitrogen, Carlsbad, CA, USA) was used for the expression of fusion proteins with V5 and 6 × His tags.

Plasmid construction for dsRNA feeding

Plasmids were constructed as described previously.[68] Briefly, the sequences encoding *ecSODs* genes were inserted into the RNAi vector L4440, containing two convergent T7 polymerase promoters in opposite orientation separated by a multiple cloning site.

Preparation of dsRNA and dsRNA feeding

The plasmids for dsRNA feeding were transformed into the bacterial host *Escherichia coli* HT115 (DE3). In brief, a single colony of HT115 containing the recombinant L4440 vector was inoculated into 4 mL of LB medium containing 4 μL ampicillin (100 μg/mL) and 4 μL tetracycline (100 μg/mL) and cultured overnight at 37°C. The cultures were diluted to reach an OD_{600} of 0.4. Isopropyl-β-D-thiogalactopyranoside (IPTG) was then added at a final concentration of 0.8 mM, and the cultures were incubated for 4 h with shaking at 37°C. An aliquot of the suspension (200 mL) was centrifuged at 10,000 × *g* for 10 min; the pellet (OD_{600} ≈ 1) was resuspended in 5 mL of sterile H_2O after cooling to 50°C and mixed with 50 mL of freshly prepared artificial feed. The prepared dsRNA feed was stored in a small plastic box (9.5 × 7.0 × 5.5 cm, 200 mL) at 4°C and used within one week. Control *S. litura* received a standard feed. Before hatching, *S. litura* eggs were placed on artificial food. For long-term maintenance of the dsRNA diet, larvae were provided with fresh food every day.[69] Hemocytes were harvested on day 7 for ROS detection. Head capsule measurement was performed daily using the OPLENIC software. Cocoon formation and eclosion of *S. litura* were analyzed. *EGFP* dsRNA was used as a control dsRNA.

Western blotting

Western blotting was performed as previously described.[67] Briefly, the cultured cells were lysed using RIPA lysis buffer (cat. no. R0100; Solarbio, Beijing, China), and the protein concentrations were measured using a BCA protein quantification assay kit (cat. no. BCA02; Dingguo, Beijing, China). Samples (50 μg) were separated by SDS-polyacrylamide gel electrophoresis and transferred to PVDF membranes. After incubation with antibodies, the bands were visualized using enhanced chemiluminescence (Beyotime).

Real-time qRT-PCR

Total RNA was isolated from samples using RNAiso Plus (9109, TaKaRa, Dalian, China), according to the manufacturer's instructions, followed by DNase treatment. The mRNA was reverse-transcribed and quantified using a 5× All-In-One RT Master Mix Kit (abm, Vancouver, Canada). EvaGreen 2× qPCR MasterMix (Abm, MasterMix, Richmond, Canada) was used for qRT-PCR on a QuantStudio and 7 Flex PCR system (ThermoFisher Scientific). Analysis for each sample was repeated three times. The relative gene expression was calculated by the $2^{-\Delta\Delta CT}$ method.[70]

Immunofluorescence

Immunofluorescence was performed as previously described,[67] with minor modifications. High Five cells were cultured on glass coverslips to 80% confluency, fixed with 4% paraformaldehyde, and permeabilized with 0.2% Triton X-100. Non-specific sites were blocked with 4% milk. Subcellular localization of ecSODs was detected with a custom-made mouse monoclonal antibody against ecSODs-V5 (Thermo Fisher) followed by Alexa Fluor 568 goat anti-mouse IgG (Beyotime). Subcellular localization of Inxs was detected with rabbit polyclonal anti-Inxs and anti-connexin 43. and Alexa Fluor 647 goat anti-rabbit IgG (Beyotime). Cells were counterstained with DAPI, and the coverslips were mounted onto glass slides for viewing with a Leica time-real scanning microscope.

Dye uptake via hemichannels

Dye uptake was performed as previously described,[2] with minor modifications. Cells were incubated with TO-PRO-3 (Thermo Fisher, T3605, Eugene, OR, America) for 15 min at room temperature. Five images were recorded per plate using the 20× objective lens (both bright and fluorescent fields) of an inverted fluorescence microscope (Olympus 1X71) at room temperature.

Detection of proteins in the cell membrane

Membrane proteins was detected as previously described,[67,71] with minor modifications. Membrane proteins were extracted from Spli221 cell pellets incubated with a condition medium containing ecSODs using the Minute Plasma Membrane Protein Isolation and Cell Fractionation Kit (SM-005, Invent Biotechnologies, INC, Beijing, China) according to manufacturer's instructions. Ectopic V5-fusion ecSOD proteins were detected using antibodies as previously described in the section of western blotting.

Co-immunoprecipitation and immunoblot assay

Cell lysates were collected and lysed with RIPA lysis Buffer (P0010, Solarbio, Beijing, China) and PMSF (P0100, Solarbio, Beijing, China) (RIPA:PMSF = 100:1). Lysates were incubated with an antibody and protein A/G agarose (P2012, Beyotime, Shanghai, China) overnight at 4°C. The precipitated protein complex was harvested and subjected to immunoblot assay.

Prediction of functional domains

Modeling of ecSODs from the wasp *M. bicoloratus* was performed using the SWISS-MODEL website (https://swissmodel.expasy.org) and Phyre[2] (http://www.sbg.bio.ic.ac.Uk/phyre2/html/page.cgi?id = index); motifs were analyzed using the Motif Scan (https://myhits.sib.Swiss/cgi-bin/motif_scan).

Neighbor joining (NJ) phylogenetic tree construction

The gene sequences of 28 different ecSOD3 from 25 different species from *M. bicoloratus* to *Homo sapiens* and Cu/Zn SOD1 from *Homo sapiens* were downloaded from the NCBI gene database[72] (https://www.ncbi.nlm.nih.gov/gene/?term=). The accession numbers of all downloaded sequences are listed in Table S1. The FASTA file was analyzed using Bioedit[73] and MEGA7.0,[74] and the systematic cluster tree was constructed using the NJ method. The protein sequence logo was constructed using WebLogo[75] (https://demo.tinyray.com/weblogo).

QUANTIFICATION AND STATISTICAL ANALYSIS

The data were analyzed using GraphPad (ver. 9.5.1, Prism), and statistical significance was examined using unpaired t-test. $p < 0.05$ was considered a significant difference between groups. The data are presented as mean ± SEM from at least three independent experiments.